

# **Debris-Flow processes in the Illgraben**

Masterarbeit

der philosophisch-naturwissenschaftlichen Fakultät

der Universität Bern

vorgelegt von

David Schnydrig

2007

Prof.Dr., Fritz, Schlunegger Institut für Geologie

## **Debris-Flow processes in the Illgraben**

**David Schnydrig<sup>1</sup>, Marco Schwab<sup>1</sup>, Dirk Rieke-Zapp<sup>1</sup>, Fritz Schlunegger<sup>1</sup>,  
Klaus Budmiger<sup>2</sup>**

<sup>1</sup>Institute of geological sciences, University of Bern, Baltzerstrasse 1-3, CH – 3012 Bern, Switzerland

<sup>2</sup>Flotron AG, K., Budmiger, Gemeindemattenstrasse 4 CH – 3860 Meiringen, Switzerland

## 0. Abstract

The Illgraben is known as one of the most active debris flows in the Alps. Many investigations have been carried out in this torrent to better understand the behaviour of debris flows. For this reason many data from different measuring installations, including a force plate in the lowermost part of the channel, are available to determine e.g. the total sediment flux during a year. Unfortunately these data include just information about the torrent since the year 2000. It was a point of interest to perform an approximate sediment budget for the Illgraben catchment over the last decades in order to see how the Illgraben and therewith probably also other torrents in the Alps have developed in these times. To achieve this goal, digital photogrammetry has been performed to determine discharge over a time span of forty-five years. To construct two digital elevation models and calculate the mass difference, a segment in the catchment with presumably high erosion rates has been digitized. This area was identified through optically compared images taken at different years. For different reasons that are later elucidated, it was not possible to digitize neither the complete catchment area nor the entire active area. Nevertheless the buildup of a sediment storage in the upper part of the channel could be identified. This implies that more sediment was eroded in the catchment and supplied to the channel than was exported to the trunk stream (i.e. the Rhône). The determination of the petrographic composition of the clasts allowed to allocate the distinct sediment source in the catchment. Furthermore we found out, that the discharge of the torrent is in the same order of magnitude over the last forty five years compared to the data of the force plate that considers a span of time of four and a half years (2000 – 2004). The ‘active’-area in which we suppose highest sediment yields delivers about 80 000 m<sup>3</sup> of mass per year. This volume can be compared to 60 % (72 000 m<sup>3</sup>) of the measured volume (120 000 m<sup>3</sup>) of the force plate, because about 60 % could be allocated to this part of the catchment.

On the aerial photographs it is recognizable that the shape and the flow pattern of the Rhône changes where the confluence of the Illgraben is located. For the exploration of potential controls, we analyzed 4 bedload samples of the Rhône for the grain size distribution. Two sites are located above and two beneath the confluence of the Illgraben with the Rhône. Furthermore a longitudinal stream profile of the Rhône was constructed. The sediment beneath the confluence showed a much coarser distribution and the channel gradient of the Rhône is much steeper there. Above the confluence, oxbow lakes that are

aligned with a high sinuosity and that exhibit scroll bars in the inner side of the meander loop imply a meandering flow pattern before the first Rhône-correction was completed between 1863 and 1893. This shows the direct influence of sediment discharge from the Illgraben on the flow pattern, stream gradient and grain size distribution of the Rhône.

## 1. Introduction

Debris flows are frequent processes in the Swiss Alps and a couple of events have produced significant damage and fatalities during recent decades (e.g., Rickenmann and Zimmermann, 1993; Zimmermann, et al. 1997a). After the catastrophic debris flows of 1987, a comprehensive study was carried out on debris-flow type, source area geology, debris-flow volume, and rainfall thresholds for debris-flow initiation (VAW 1992). In recent years, research has focused on laboratory experiments and numerical simulations (Rickenmann and Koch, 1997, Rickenmann and Weber, 2000, Tognacca 2000). Furthermore, three debris-flow observation stations were installed in Switzerland. Two of them (Dorfbach and Schipfenbach) were completed in summer 1997. The third observation site comprises the catchment of the Illgraben that is a ca. 9.5 km<sup>2</sup>-large tributary of the Rhône-river in the Central Alps of Switzerland. This Illgraben debris flow system with an annual sediment discharge of ca. 100000 m<sup>3</sup> represents one of the most active torrents in the Alps. It was in the year 2000 when multiple survey instruments including geophones, radar, laser, ultrasonic depth-measuring devices, video cameras, three rain gauges and a debris-flow force plate were installed and maintained by the Swiss Federal Research Institute for Forest, Snow and Landscape (WSL). However, despite the abundance of high-resolution information about the physical properties of single debris flow events that have been recorded by this station (normal and shear stresses, pore fluid pressure, flow velocity and thickness) (McArdell et al., 2007), there are no detailed data on sediment discharge over longer time-scales (several tens of years), nor is there quantitative information about the location of the sediment source. This information will be partly delivered in the framework of this study.

The aim of this paper is the allocation of the sediment sources and the quantification of the magnitudes of discharge from the source to the valley. In addition, special attention was focused on the identification of potential effects of sediment discharge on the morphology of the Rhône valley. The data are elevation differences in the

catchments between 1959 and 2004 that were extracted from aerial photographs using standard photogrammetric techniques. This method allows to identify the locations of potential sediment sources, sinks and segments of sediment transfer. The implication of sediment discharge for the morphology of the Rhône valley is based on sedimentological data including sedimentary petrography and analysis of channel morphologies.

## **2. Setting**

### **General Setting**

The ca. 9.5 km<sup>2</sup>-large Illgraben catchment represents a tributary system of the Rhône valley and is located in the Central Alps of Switzerland (Fig. 1). The highest summit is represented by the Illhorn with an elevation of 2717 m a.s.l., and the lowest location is the point of entry of the Illgraben into the Rhône river at 610 m a.s.l. Hence, the relief of the catchment measures ca. 2100 m. The bedrock is part of the Penninic nappes and comprises low-grade quartzites in the southern part of the catchment, low-grade marbles, rauwackes and dolomites on the northern flanks and schists along the feeding channel (Fig. 2). Approximately 50% of the catchment is drained by the Illbach with the Illsee hydropower reservoir in the higher segment of the drainage basin, where no debris flows have been reported. The other portion of the catchment is drained through the Illgraben. This part of the catchment has been the debris flow source area (Gwerder, C., 2007).

### Geographical position of the Illgraben torrent

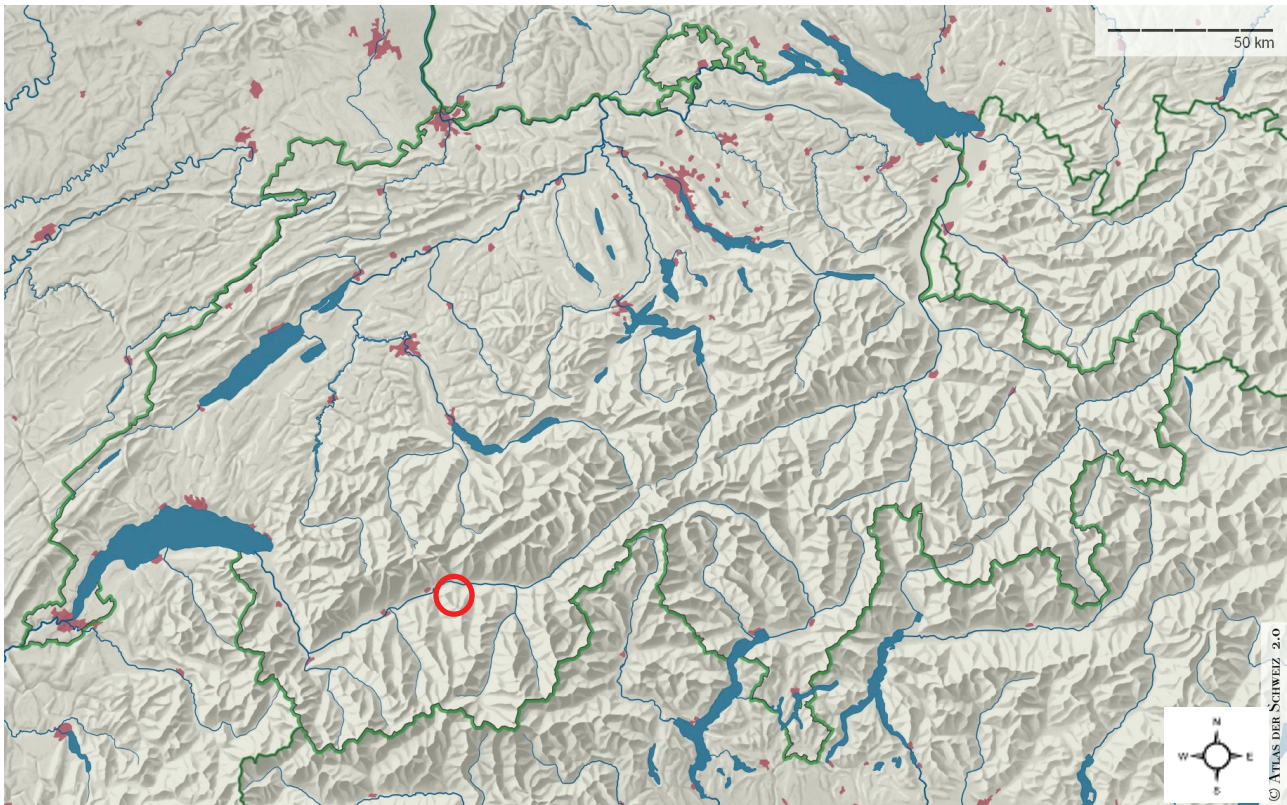


Figure 1: The Illgraben is located in the central Alps and is a southern tributary of the Rhône (Atlas der Schweiz 2.0).

### Lithology of the Illgraben catchment

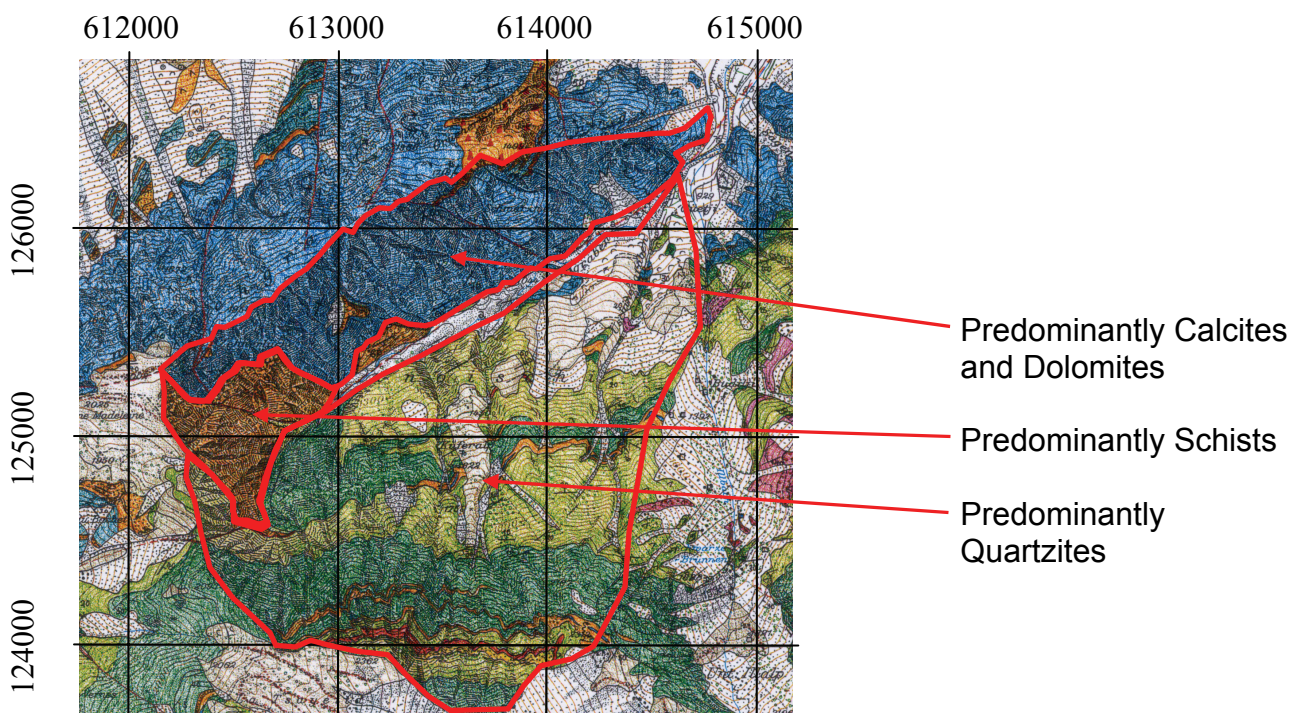


Figure 2: Geological overview of the Illgraben catchment (Geological map is in the Appendix).

The topography of the Illgraben catchment is made up of 44 % of exposed bedrock, whereas 42 % and 14 % of the basin is covered by forests and grass, respectively (Gwerder, C., 2007). As noted above the bedrock geology comprises alternated quartzite beds and calcareous sedimentary rocks on the south-eastern part of the basin, and cliffforming walls of dolomite beds on the northwest fall. The dolomites are unusually susceptible to physical weathering and provide a large amount of silty material. In addition, these deposits are strongly jointed and have repeatedly caused rock falls. For instance, in 1961, a large rockfall released a total of  $3 \cdot 10^6$  to  $5 \cdot 10^6$  m<sup>3</sup> of material to the Illgraben channel, which, in turn, was an important source for successive debris flows. A further important source of material has been the quartzites in the south-eastern segment that have released material to the Illgraben channel by mass failure (Hürlimann, M. et al. 2003).

The Illgraben catchment is situated in an interalpine valley, and the climate is therefore strongly influenced by this geographical position. This climate is characterised by a low annual precipitation and mild annual average temperatures. The annual precipitation rate is about 700 mm in the lower part of the catchment and ranges to 1700 mm at the highest parts (Swiss Federal Office for Water and Geology 1999; Hürlimann et al. 2003). Intense rainstorms with estimated magnitudes between 35 and 57 mm/h for a 0.5 to 1 h rainfall duration, respectively, mainly occur in summer. These magnitudes correspond to a return period of approximately 100 years (Swiss Federal Office for Water and Geology, 1999; Hürlimann, et al., 2003).

Different constructional techniques were applied to control the torrent. At about 1000 m a.s.l. a grand debris flow retention dam of about 50 m height was constructed between 1967 and 1969 to protect the area in the valley. Further downstream of this large dam, a series of smaller check dams decrease the gradient of the torrent and try to take kinetic energy out of the channel (Hürlimann et al., 2003).

There exist historical data on the debris flow activity of the Illgraben from the beginning of the 20<sup>th</sup> century. They show that debris flows have occurred regularly during the last hundred years. Many events with magnitudes less than 75 000 m<sup>3</sup>, five events with volumes ranging from 75 000 to 250 000 m<sup>3</sup> and one event in 1961 with a total volume of about 500 000 m<sup>3</sup> of transferred material are included (GEO7, 2001, Hürlimann et al., 2003). Interestingly, the large rockfall event in 1961 significantly increased both the magnitudes and frequencies of the debris-flow activities in the succeeding years. It was in the 1970s when the debris-flow frequency decreased on the fan due the construction of

the solid gravity dam in the middle reach of the torrent. However, by the early 1980s, this ca. 50 m high sediment retention dam was filled, and debris flow activities reached the long-term magnitudes and frequencies during the last 20 years (Hürlimann et al., 2003).

### **Instrumentation**

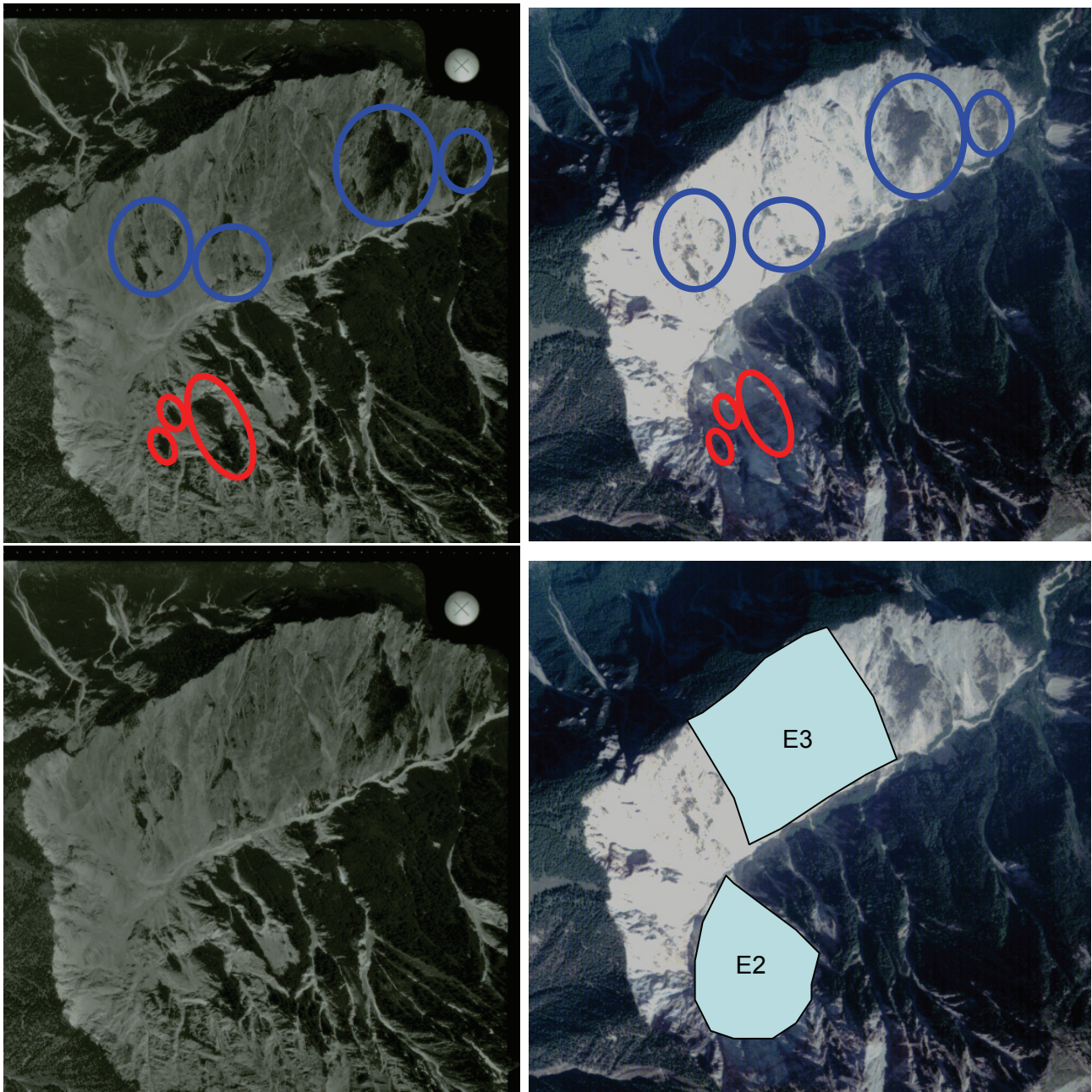
The WSL-survey stations are equipped with multiple measuring instruments and installations including video cameras for the recording of debris-flow waves. The recordings can be used to make statements about the flow behaviour and the geometry of the wave. Furthermore it is possible to get information about the material composition, the water content and potential wood in the debris flow (Rickenmann et al., 2001). Radar, laser and ultrasonic measuring devices are needed to measure the discharge-depth relationship and to construct a detailed longitudinal profile of the front wave. These measurements are also helpful for a semi quantitative analysis of the video recordings (Rickenmann et al., 2001). On one hand, the geophones serve as a release survey instrument for the automatic start-up of all the other instrumentations, and on the other hand it is possible to make propositions about the pass moment of the front wave and about how intensity of the debris flow develops during its passage. The combined information of several geophones and/or fathometers allows calculating the frontal velocity of the flows (Rickenmann et al., 2001). The rain gauge stations measure the rain intensity before and during an event, so that threshold conditions for flow initiations are known (Rickenmann et al., 2001). The force plate measures the weight and the shear stress of a continuous debris flow. Together with the depth-measurements these data allow to calculate the debris flow's density (Graf and McArdell, 2004). Finally, pore water pressures are measured. These data serve as crucial parameters for understanding flow dynamics (Graf and McArdell, 2004).

### **3. Methods**

#### **Digital photogrammetry**

The allocation of sediment sources and the quantification of the magnitudes of sediment transfer in the Illgraben catchment during the last fifty years was performed using the technique of digital photogrammetry. Before this technique was applied, optical comparisons of the multitemporal aerial-photographs were made to search out the most active areas, in terms of landscape change (Fig. 3, E2 & E3). The area E2 has been recognised as the most active area and is situated in the south-eastern catchment (Fig. 3). The area E1 was used as a test area and is not considered in this thesis. E3 is the area in the south-western catchment and could not be used for quantitative calculation. The reasons for this will be discussed later. The photogrammetry allows extraction of topography at the time the images were taken. The task is to establish the geometric relationship between the image and the reality at the time of imaging (Mikhail et al., 2001; Schwab et al., in press). Two high-resolution Digital Elevation Models (DEMs) were extracted and compared. This was accomplished partly by automatic and partly by manual collection of elevations from aerial photographs. The differences between these models yielded information about the change of the topography and hence about magnitudes of sediment transfer between the time intervals of image acquisition. It provided data about the change in elevation in the debris flow and rock fall area and therefore about the volumetric redistribution of the landmass by these processes. The difference between removed and accumulated volume corresponds then to the volume of sediment that became exported from the system. Note that this technique was successfully applied in rock-glacier surveys to detect changes in glaciated areas (Kääb, 2002; Kääb et al., 2005) and also on landslides (Gentili et al., 2002; Schwab et al., in press).

### Optical comparisons of the catchment with the aid of multitemporal aerial photographs



Aerial photograph of 1959

Aerial photograph of 2004

Figure 3: E2 and E3 are areas of manual digitalization. Difference models follow in Figure 4 and 5.

- No changes visible
- Changes visible

For the Illgraben area, we ordered the oldest (1959) and the most recent images (2004) that are currently available to retrieve data for the largest possible time span. These images were scanned with the photogrammetric scanner VEXCEL UltraScan 5000 (Gruber and Leberl, 2001), with a resolution for the old images of 600 to 2400 dpi and for the new images of 2400 to 3200 dpi. This corresponds to the flying height and to the quality of the paper images (Schwab et al., in press). Note, however, that the resolution of the 1959 images was poorer than that of the most recent ones. The processing of the images was performed on a Digital Photogrammetric Workstation (DPW) running the software Leica Photogrammetry Suite (LPS v9.0). The calibration protocols for the different images were taken from Swisstopo. Note that each stereo-block required different protocols for the corresponding camera (Appendix). This information was then used to perform the interior orientation. In a further step, the exterior orientation of the camera was calculated by resection in space. This was done using control points that were measured with a differential GPS for the area that was covered by the stereo images. The criteria for point-selection was that each point could be unequivocally identified in all images, even in the older ones. This strategy substantially restricted the number of possible target points as numerous well-recognizable features (e.g., road intersections) changed through time. 19 Ground Control Points could be identified in both picture age-groups. 284 tie points were identified in the old images and 69 in the new ones. These points were found partly automatically and partly manually.

The root mean square error given after the triangulation was 1.16 pixels. This is the internal precision of measurements in the image. Measurements cross-check with check points and stereo measurements on the Digital Photogrammetric Workstation showed deviation in the range between 0.37 and 0.50 m. The extraction of the three dimensional information was then performed using automatic tools offered by LPS and manual editing tasks using stereo visualisation.

For the extraction of mass points different default strategy parameters ("High Mountains", "Rolling Hills" and "Forest") offered by LPS were tested (Gooch et al., 1999) proposed an accuracy assessment of DEMs generated by the software. They tested the effect of the parameters that controlled the search and the quality control of the algorithm. The search window for automatic point identification was adapted from the default strategies representing surface topography ('high mountains') and applied to specific zones. Nevertheless, the results could not be used directly for a surface analysis in the debris flow source area because there were too many wrong results. The pictures of 2004

were taken between 09.45 and 10.15 am and have therefore shadows in many parts in the active area, which make digitalization very difficult in those areas. In addition it was impossible to see the morphology from the same perspective in the two sets of aerial photographs. Similarly, details in the geometry of the feeding channels could not be digitized with sufficient resolution (Fig. 5). These drawbacks made a digitalization of some parts of the active area impossible and an extrapolation had to be made (Fig. 4). Finally, most of the points were extracted manually, and in addition breaklines were digitized. DEMs were then generated in the program ERDAS with different grid sizes (1 m, 3 m, 5 m). On a test area where no mass movements have occurred during the last 45 years, points and breaklines were digitized in order to test the consistency of DEM extraction. Specifically, differences between DEMs are anticipated to yield the topographic change in these particular regions. All DEMs were then exported to ArcGIS 9 (ESRI Inc, 2004) and the old ones were then subtracted from the new ones. The test areas yielded the smallest errors when a grid size of 1m was chosen. Error calculations in this test area also illustrated that sites with a mass difference smaller than +/- 2 m should not be considered. These ones are not illustrated on Figures 4 & 5.

### Difference Model 1

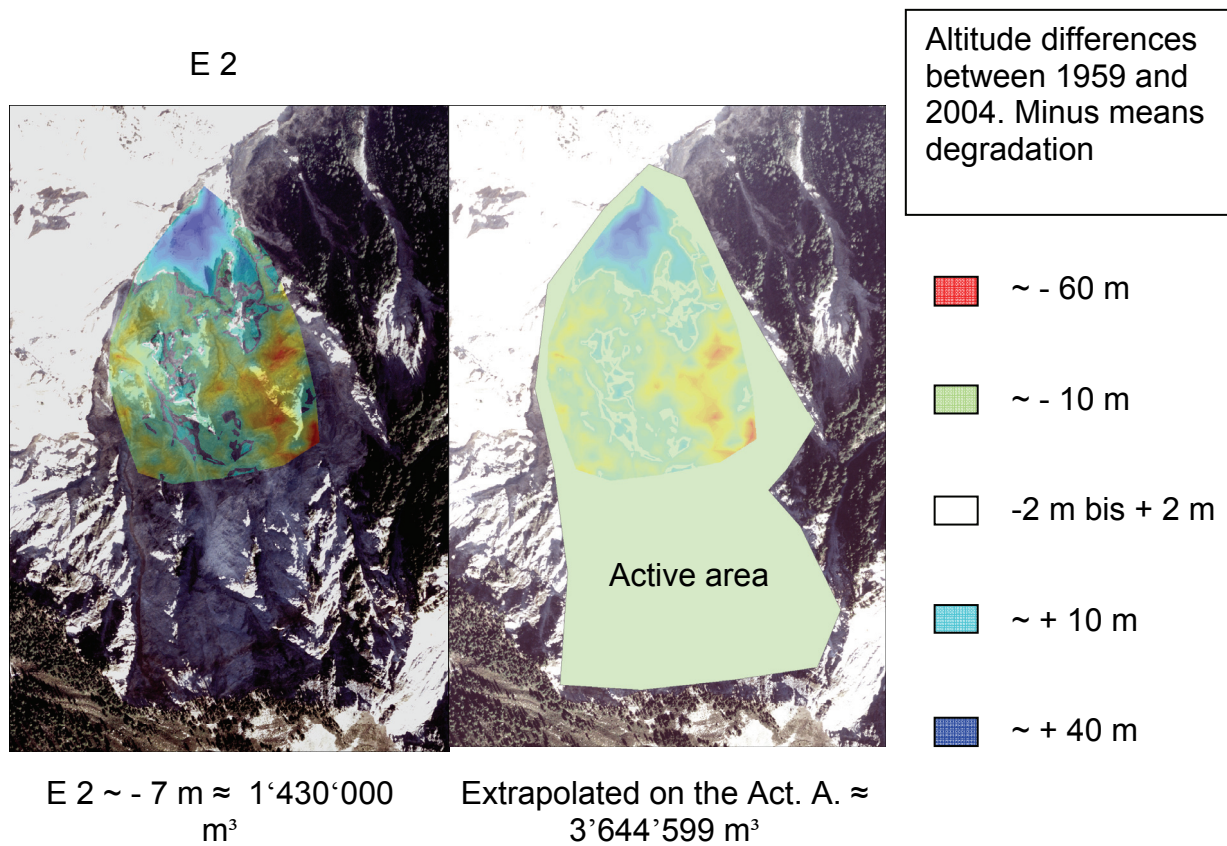


Figure 4: Degradation of the digitized area E2 and an extrapolation on the active area where a similar high degradation is expected (Table 1).

## Difference Model 2

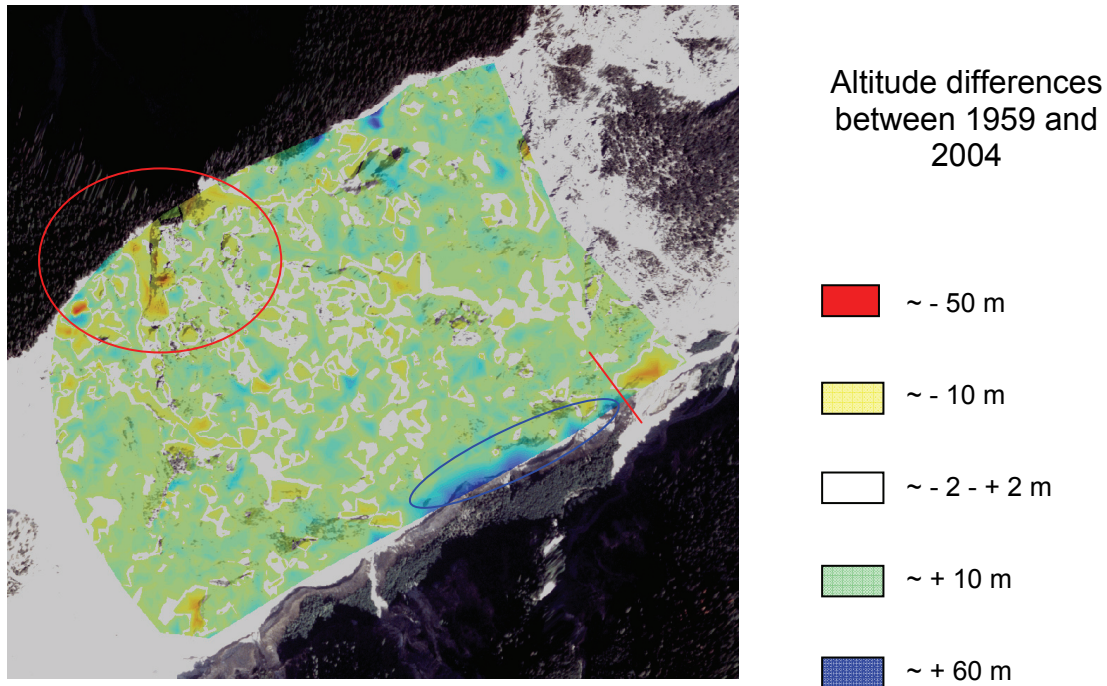


Figure 5: Digitized area E3 where problems inhibited a quantitative analysis.

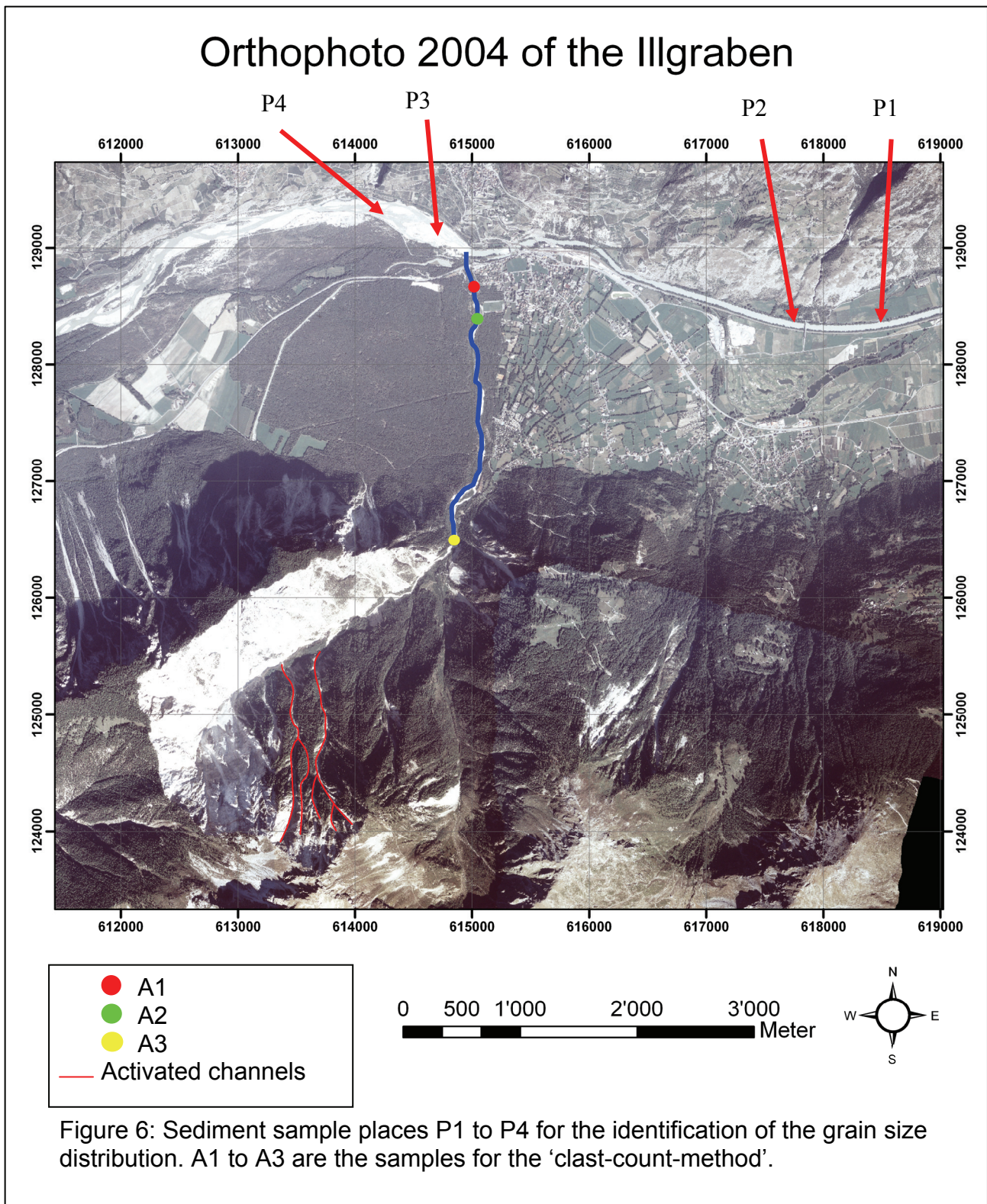
- Possible source of the large rockfall in 1961
- Sediment accumulation behind the large retention dam
- Location of the retention dam

In 2000 different instrumentations were installed, that have been supervised by the WSL, in order to the debris flow events. Since the installation of this monitoring system, it has been possible to measure the velocity, the maximum high, discharge and the total volume of an event. One of the goals of this paper is to compare this quantified total volume of the last four and a half years with the volume lost over the last 45 years. Therefore different areas in the catchment were digitized on the aerial photographs of 1959 and 2004. The mass lost could then be calculated by subtracting the two models. The sum of the Z-values of every point then yields the mass balance of exactly this area. Because of the problems with the automatic DEM generation, only the areas E2 and E3 in

the catchment could be digitized (Fig.4 & 5).

### **Sedimentary petrography**

The lithology of the catchment is well known. As outlined above the northwestern catchment consists mainly of rauwackes, dolomites and limestones. The southeastern catchment is mainly made up of quartzites, as well as schists and gneisses in the southwestern portion where the channel starts. To estimate the contribution of these segments to the sediment budget of the whole catchment, the 'clast-count-method' was applied at three different locations. In each of these sites 300 clasts were collected from an area of 1m<sup>2</sup> and quantitatively attributed to different lithologic types (Fig. 6). This allowed to estimate the relative contribution of the various portions in the catchment to the sediment budget (Fig. 9.1 to 9.3).



## **Sedimentology and geomorphology**

One goal of this thesis was to explore the effects of sediment discharge from the Illgraben on the morphology and sedimentology of the Rhône valley. Accordingly, a longitudinal stream profile of the Rhône river was reconstructed based a high-resolution topographic map (1:25 000, Sierre, Swisstopo, Fig. 7). The rational behind this approach lies in the general findings that any non-linear relationships in the sediment budgets between tributary and receiving trunk stream will ultimately influence gradients and curvatures of the main river. Additionally four bedload samples of the Rhône-river were analyzed for the granulometric composition of the bedload. Two samples were taken each above and beneath the confluence of the Illgraben with the Rhône (Fig. 6). The samples were sieved using standard sedimentological techniques (Krumbein & Pettijohn, 1961; Folk, 1974b; Buller & McManus, 1979; Fig. 8). The rational behind this strategy lies on the findings by McManus (1988) that the size of the component particles is one of the fundamental textural characteristics of the fragmentary deposits and their lithified equivalents.

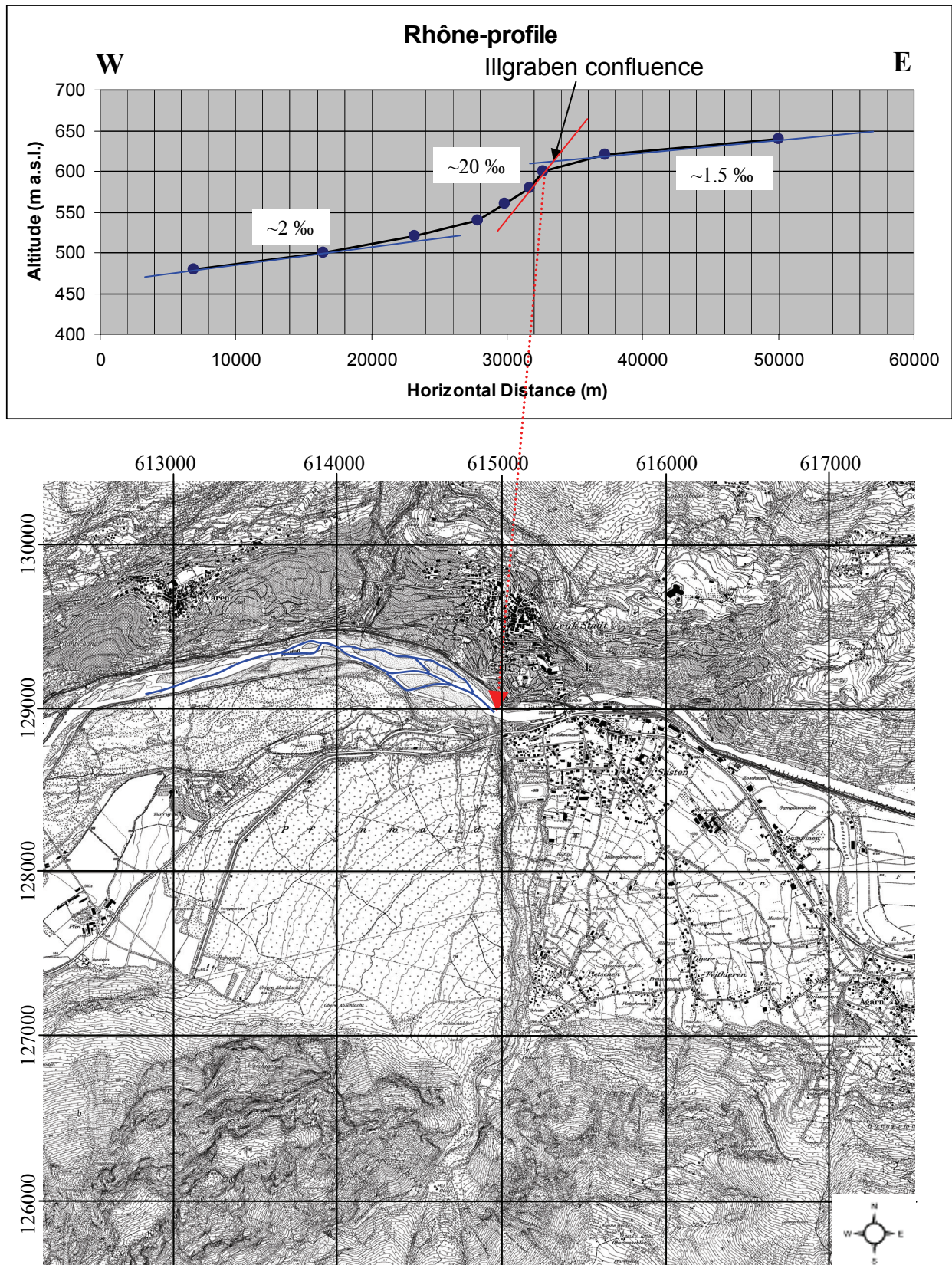


Figure 7: Rhône profile with inflection point and change in flow-pattern of the Rhône in the area of the Illgraben confluence.

~ Braided flow pattern beneath the confluence of the Rhône with the Illgraben.

**Grain size distribution curves of the sand samples that were taken in the Rhône channel (Cumulative Frequency Curves)**

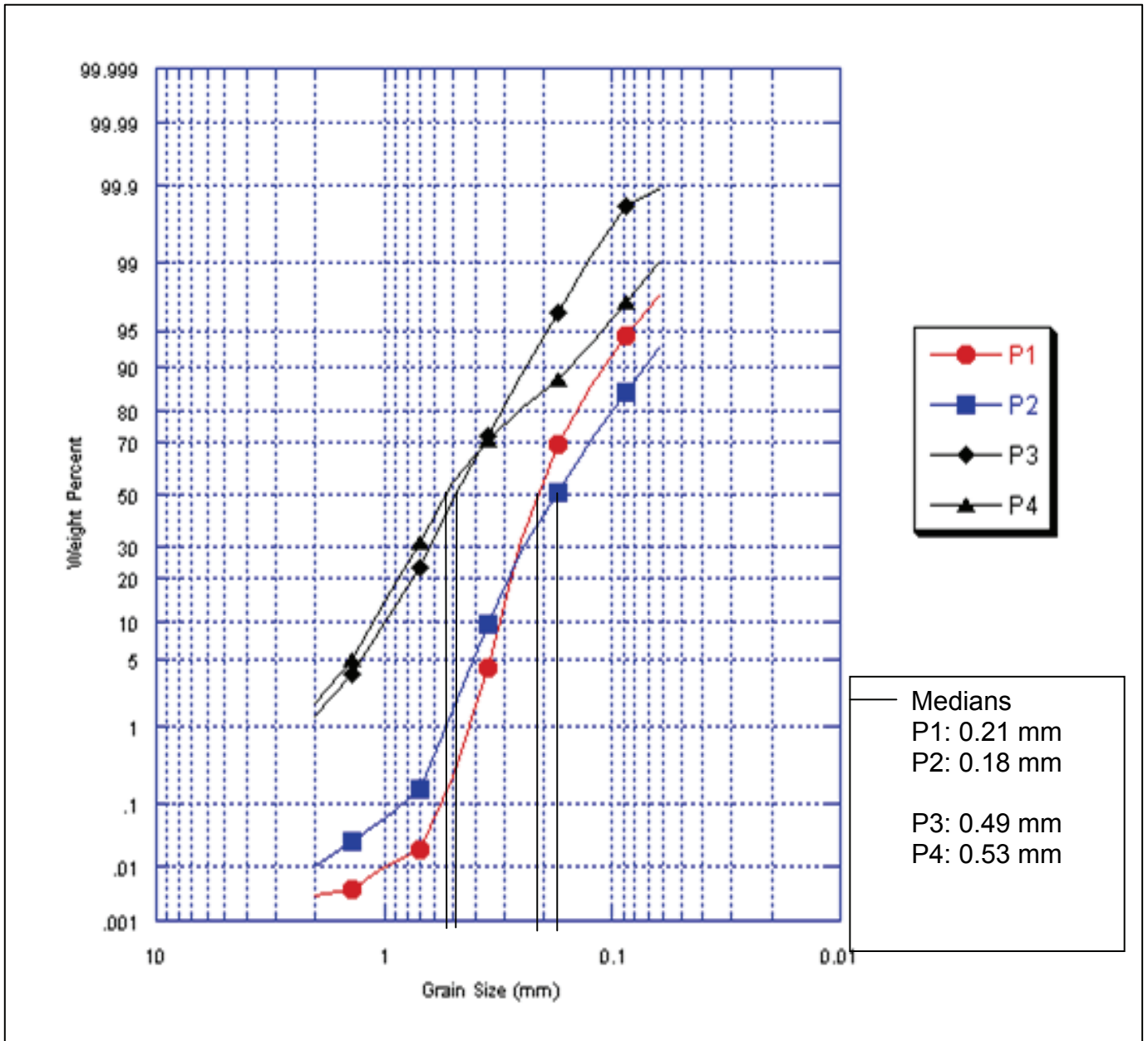


Figure 8: P1 and P2 are located above the confluence of the Illgraben and are much finer-grained than P3 and P4 that are located below the confluence. Overview of the sample locations in Figure 6.

Galloway and Hobday (1983) proposed a model that shows a consistent relationship between the flow pattern of a river and the relative importance of bedload. Specifically, an increase in the bedload/total load ratio (bed load plus suspension load) tends to promote unconfined flow conditions (braided river). Because sediment discharge by the Illgraben potentially changes the granulometric composition of the mechanical load of the Rhône and thus the flow pattern, we mapped the facies of the Rhône valley using classical tools in process sedimentology (Schlunegger et al., 1993).

## 4. Results

### Digital photogrammetry

A calculation of the most active area E2, located in the south-eastern catchment, was made in ArcGis (Arcmap) (Fig. 3 & 4). The rockfall area E3 in the north-western catchment was not considered in the calculation due to problems that are discussed later (Fig. 3 & 5). The 1959 DEM was subtracted from the one of 2004. The average degradation of the 205 000 m<sup>2</sup>-wide E2 over the time span of 45 years is about 7 m, which corresponds to a mass lost of about 1 400 000 m<sup>3</sup>. When area E2 is extrapolated over the circa 520 000 m<sup>2</sup>-wide 'active'-area, a mass lost of about 3 600 000 m<sup>3</sup> is received (Fig. 4, Table 1 & 2). The active area was defined through optical comparisons of the multitemporal (1959 and 2004) aerial photographs (Fig. 3). This 'active'-area then delivered about 80 000 m<sup>3</sup> of material per year over the last 45 years. The 'clast-count-method' showed that about 60 % of the material comes from the southern catchment that is also part of the active area (Fig. 9.1 to 9.3). WSL-data from 2000 to 2006 showed an average discharge of about 120 000 m<sup>3</sup> per year (Table 2). 60 % of this volume are 72 000 m<sup>3</sup> and are in the same order of magnitude as the discharge that is measured here for the last 45 years. Note that the active area does not cover the whole area where quartzites are exposed. Therefore the calculated 80 000 m<sup>3</sup> per year represent just a minimal estimation of the discharge over the last decades. Furthermore the built-up of a sediment-storage could be recognized in lower part of the digitized area E2. This means that not all material that is supplied to the channel was transported out of the catchment and supplied to the Rhône (Fig. 4).

Mass balance of the Illgraben over the last decades (Table 1)

	Degradation	Area	Vol. deficit during 45 years	Vol. deficit during 1 year	Average measured vol. deficit during 1 y.
E2	~7m	~205 000 m <sup>2</sup>	~1 400 000 m <sup>3</sup>	~30 000 m <sup>3</sup>	unknown
Active area	~7m	~520 000 m <sup>2</sup>	~3 600 000 m <sup>3</sup>	~80 000 m <sup>3</sup>	unknown
whole catchment	unknown	unknown	unknown	unknown	~120 000 m <sup>3</sup>

Measured mass balance since 2000 (Table 2)

Year	2000	2001	2002	2003	2004	2006
Mass discharge (m <sup>3</sup> )	120 000	131 000	96 000	95 000	75 000	245 000

### Clast count method

The clasts that were counted could be allocated to different parts of the catchment due to the known lithological architecture (Appendix - Geological map of the Illgraben, WSL). The petrographic composition is illustrated in Figure 9.1. The counts indicated that more than 60 % of the debris flow material was derived from the southern catchment side, 14 % from the channel bed, and the remaining 25 % from the northern portion of the catchment. Because the southern segment comprises just about 20 % of the entire coupled system, which is about 6 % of the entire size of the catchment, only a small area produces most of the sediment. This means that 60 % of the material was derived from 6 % of the entire catchment area. From the orthophoto and the field observations, we allocated the location of the active area to the southern portion of the catchment (Fig. 3 & 4). One aspect was not considered in this 'clast-count-method'. A substantial portion of material in the channel bed is fine grained and is thus not considered here, so that the presented quantification has to be taken with care.

### Petrographic distribution of the clasts

Clasts allocated to different segments of the catchment

Average values from the sum of A1 to A3 (Fig.6)

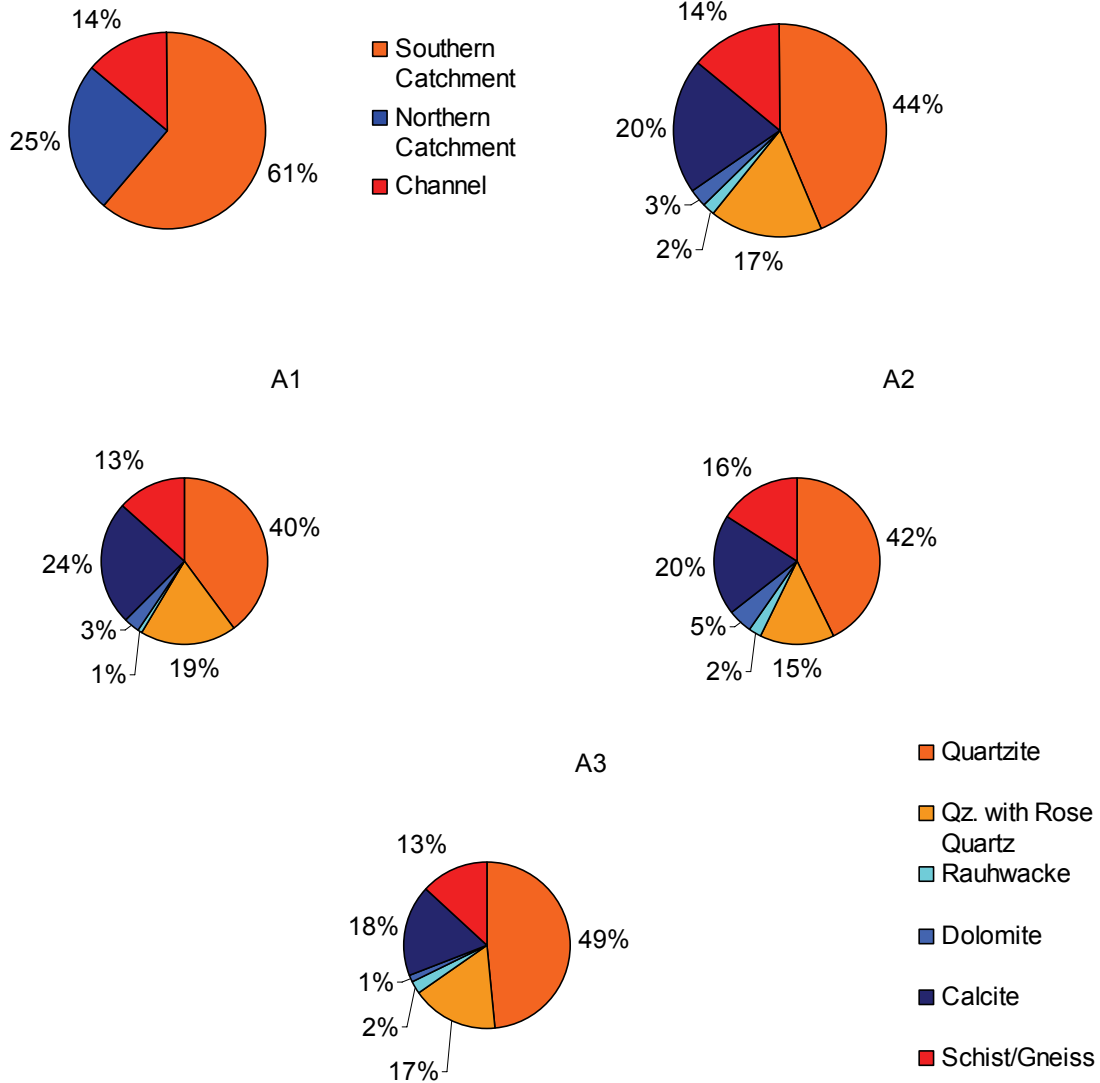


Figure 9.1: Results from the 'clast-count-method' and the allocation of these clasts to different segments of the catchment.

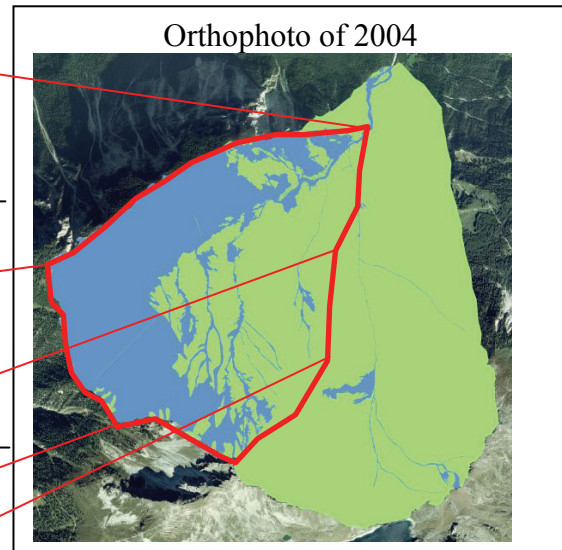
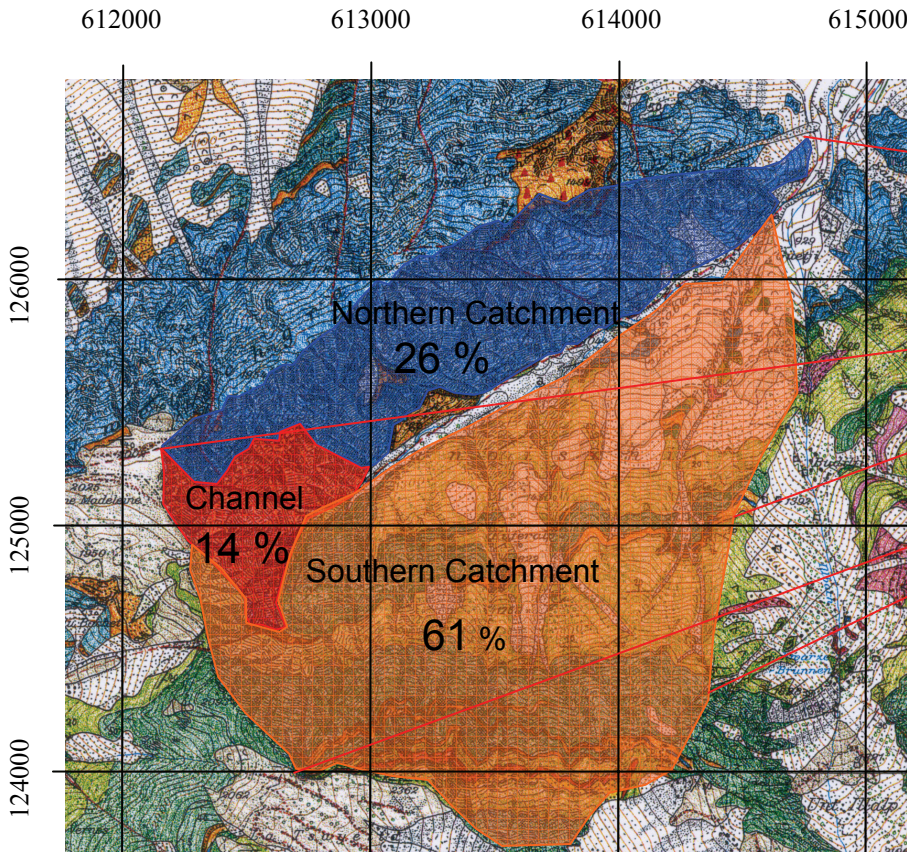


Figure 9.3: Only the coupled area of the catchment supplies more than 99% of the sediment. The other areas could be uncared-for this study.

Figure 9.2: The allocation of the clasts to different segments in the catchment. 61 % of the clasts are located in the southern catchment.

- Predominantly Calzites and Dolomites
- Predominantly Schists
- Predominantly Quartzites

- Directly coupled to the channel
- Decoupled area

### Sedimentology and Geomorphology

The longitudinal stream profile of the Rhône shows a clear inflection point in the area where the Illgraben discharges into the river (Fig. 7). It can thus be clearly seen that the Illgraben has a retain effect on the Rhône river with respect to sediment flux, and that the Rhône is strongly redirected to the northern part of the valley floor. At the point where the Illgraben discharges into the river, a change in the flow pattern can be observed. Beneath the intake, the Rhône river still flows in its natural state, and a braided flow

pattern with multiple channels separated by longitudinal bars can be observed. This part was not considered in the Rhône corrections because it has never caused damages

related to floods (Vischer, 2003). Above the confluence with the Illgraben, the Rhône has already been twice adjusted. The adjustment was performed the first time between 1863 and 1893 and then between 1930 and 1960. The oldest available topographic map of this area was that by Siegfried (1882-84) when the first adjustment was already completed. Therefore it was not possible to infer the flow pattern before the correction. Nevertheless, the presence of sinuoidal oxbow lakes and fragments of scrollbars on the lee-side of the lakes imply a meandering flow pattern prior to antropogenic alterations (Fig. 10).

### Orthophoto of 2004 with an oxbow lake of the Rhône

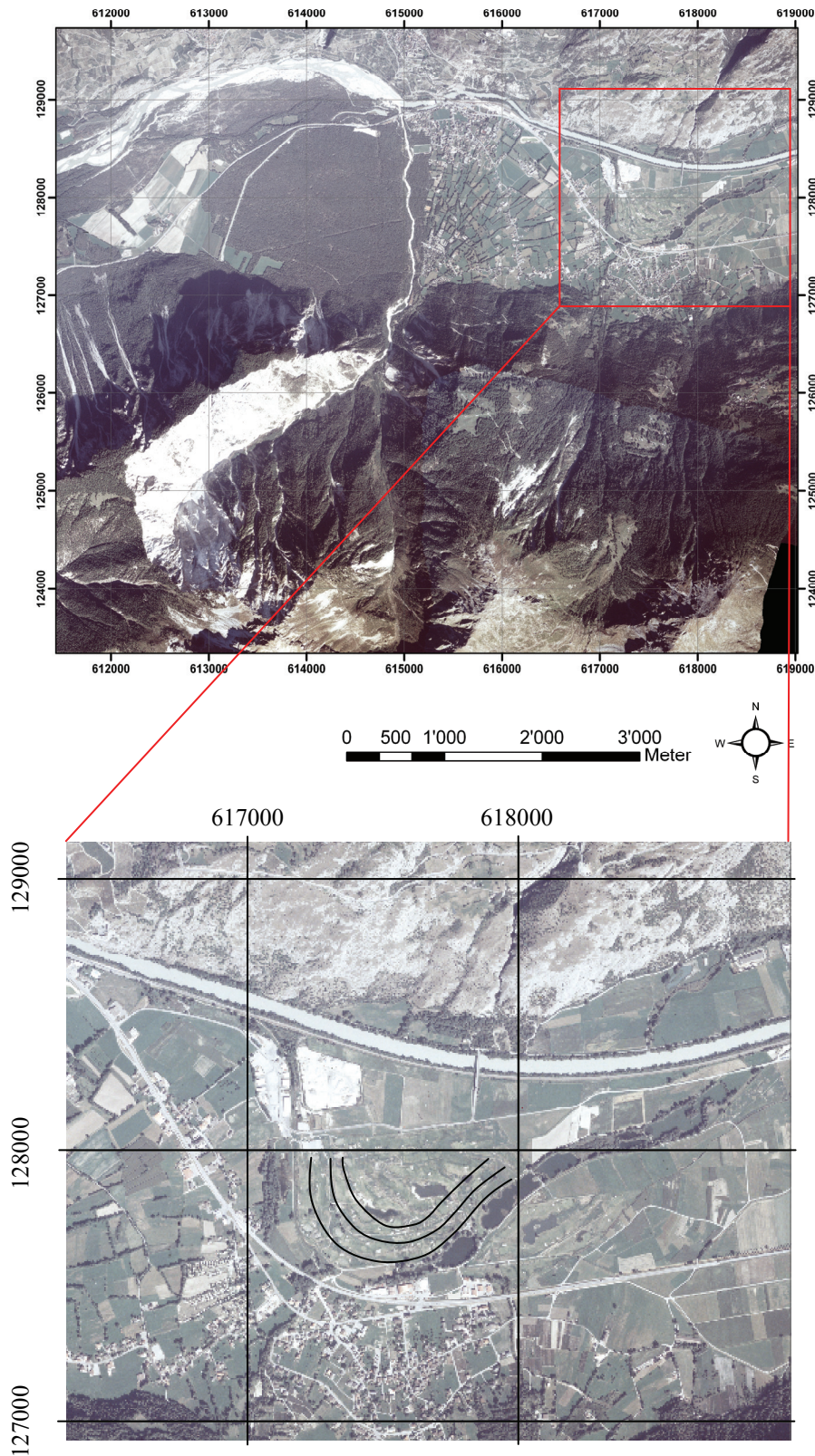


Figure 10: Oxbow lake of the Rhône shows its meandering pattern before the human impact in the end of the 19<sup>th</sup> century. On the lee side scroll bars are recognizable.

Four bedload samples were collected in the Rhône river for the assessment of the granulometric composition (Fig. 6). The two samples above the torrent intake are much finer grained than the two beneath the Illgraben (Fig. 8). The median (Md) of the samples P1 and P2, that were taken above the confluence (Fig. 6), lies in the class of 0.175 mm to 0.25 mm (Fig 8). In contrast, medians of samples P3 and P4 that were collected beneath the confluence (Fig. 6) lie in two different classes close to the border of the classes. 0.35 mm to 0.5 mm (P3) and 0.5 mm to 0.7 mm (P4) (Fig. 8). Note that the mean (M) of the samples is calculated with the formula  $Mz = \frac{1}{3} (\Theta_{16} + \Theta_{50} + \Theta_{84})$ . Further statistical parameters are presented in Table 3.1 and Table 3.2.

Statistical parameters to describe the grain size distribution (Table 3.1)

	Median (Md)	Mean (M)	Sorting ( $\sigma$ )	Skewness (SK1)	Kurtosis (KG)
P1	2.2	2.28	0.61	0.28	1.14
P2	2.5	2.58	0.87	0.17	0.93
P3	1.05	1.03	0.78	-0.03	1.03
P4	0.85	1.07	1.1	0.29	1.17

Md = 50 % of cumulative distribution curve

$M = \frac{1}{3} (\Phi_{16} + \Phi_{50} + \Phi_{84})$

$\sigma = (\Phi_{84} - \Phi_{16}) / 4 + (\Phi_{95} - \Phi_5) / 6.6$

$SK1 = (\Phi_{16} + \Phi_{84} - 2\Phi_{50}) / (2 (\Phi_{84} - \Phi_{16})) + (\Phi_5 + \Phi_{95} - 2\Phi_{50}) / (2 (\Phi_{95} - \Phi_5))$

Descriptive terms applied to parameter values (McManus, J., 1988. Table 3.2)

Sorting ( $\sigma$ )		Skewness (SK1)	
Very well sorted	< 0.35	Very positively skewed	0.3 to 1.0
Well sorted	0.35 - 0.50	Positively skewed	0.1 to 0.3
Moderately well sorted	0.50 - 0.70	Symmetrical	0.1 to - 0.1
Moderately sorted	0.70 - 1.00	Negatively skewed	- 0.1 to - 0.3
Poorly sorted	1.00 - 2.00	Very negatively skewed	- 0.3 to - 1.0
Very poorly sorted	2.00 - 4.00		
Extremely poor sorted	> 4.00		

Kurtosis (KG)	
Very platykurtic	< 0.67
Platykurtic	0.67 - 0.90
Mesokurtic	0.90 - 1.11
Leptokurtic	1.11 - 1.50
Very leptokurtic	1.50 - 3.00
Extremely leptokurtic	> 3.00

## 5. Discussion

### Implications for hazard predictions and trends

Bovis and Jakob (1999) distinguished between two different debris-flow systems. In a first case sediment flux of the system is supply-limited. This means that there is not always enough sediment available to trigger a debris-flow, even when threshold conditions for precipitation rates are exceeded. In this case, debris-flows are not predictable because sediment-storages have to recharge after bigger events, and not every heavy rainfall is able to trigger a debris-flow. In a second case sediment flux of the system is transport-limited. There is always enough sediment available in the channel that can potentially be exported. In this case the triggering of a debris-flow depends only on precipitation rates. A prediction of a debris-flow in such catchments is thus possible. For this reason we are interested in exploring if sediment discharge of the Illgraben is either supply- or transport-limited. It is also relevant to know how the trend of mass discharge has developed over a longer timescale and how it will develop in the future.

The timescale that is considered in this thesis encompasses forty-five years. In this timescale about fifty debris flow events and one large rock fall occurred. Specifically, the rock fall event in 1961 affected a total volume of about  $3 * 10^6$  to  $5 * 10^6$  m<sup>3</sup> (Hürlimann, 2002). The material of this event was released beneath the area of the drainage basin where the calcareous and dolomitic lithologies are situated and where the digitized area E3 is located (northern catchment, Fig. 3 & 5).

When the mass lost of E2 is (Fig. 3) extrapolated over the so called 'active area' (Fig. 4) where presumably highest sediment yields have occurred, and if the resulting mass balance is then compared to the mass lost of the last four and a half years, the calculated mass discharge is very similar. From historical data it is known, that no debris flow events occurred between 1966 to 1981 after the construction of the high retention wall. The wall first had to be filled with material before the sediment could be transported to the Rhône again. However, this time span in which no debris flows occurred does not affect the mass balance of the digitized area E2, because this site is located further upstream in the catchment and is controlled by other processes. When the discharge data

from 2000 – 2004 is compared to the data from 2006 (Gwerder, 2007), it can be seen that sediment discharge was substantially higher in 2006 compared to the previous time span (nearly a double fold increase, Table 2). The long term precipitation distribution in the station Sion has been constant over the last ~ 40 years (Fig. 11.1). This implies that precipitation cannot be the only reason for the increasing discharge in 2006, but temperature increased distinctly during this time period (Gwerder, 2007) (Fig. 11.2). Also, there is no evidence for an increase in precipitation intensity. Consequently, enhanced temperatures (Fig. 11.2) have had most likely an effect on the Illgraben geomorphology and sediment discharge, at least with the degradation of permafrost on the north face of the Illhorn (Gwerder, 2007). This degradation could destabilise the slopes underneath the Illhorn and provide a new sediment source. The exploration of the importance of this effect for the development of an alpine catchment, is currently a major research priority for geomorphologists (Goudie, 2006).

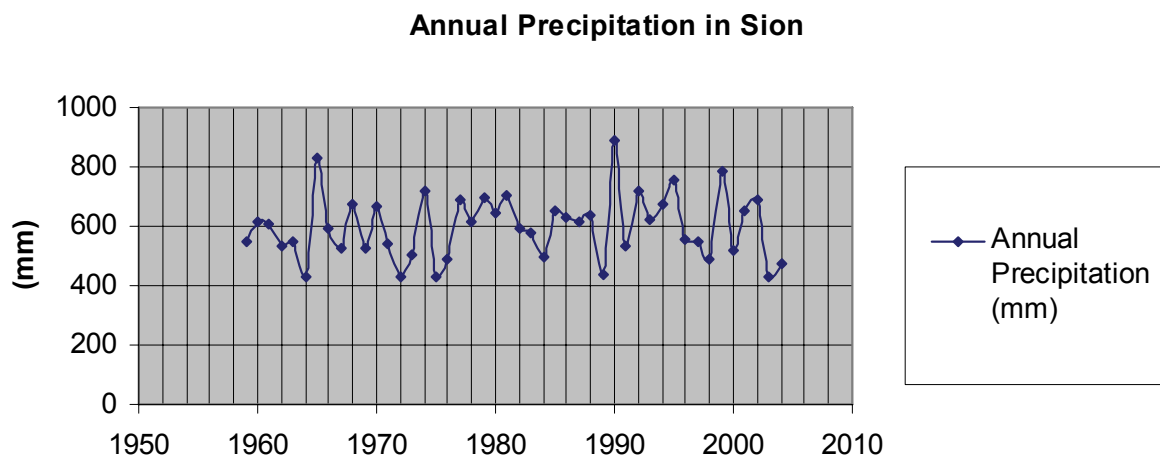


Figure 11.1.: Precipitation is very constant over the considered time span, but the variation the monthly precipitation rates seem to increase (MeteoSchweiz).

### Average Annual Temperature in Sion from 1959-2004

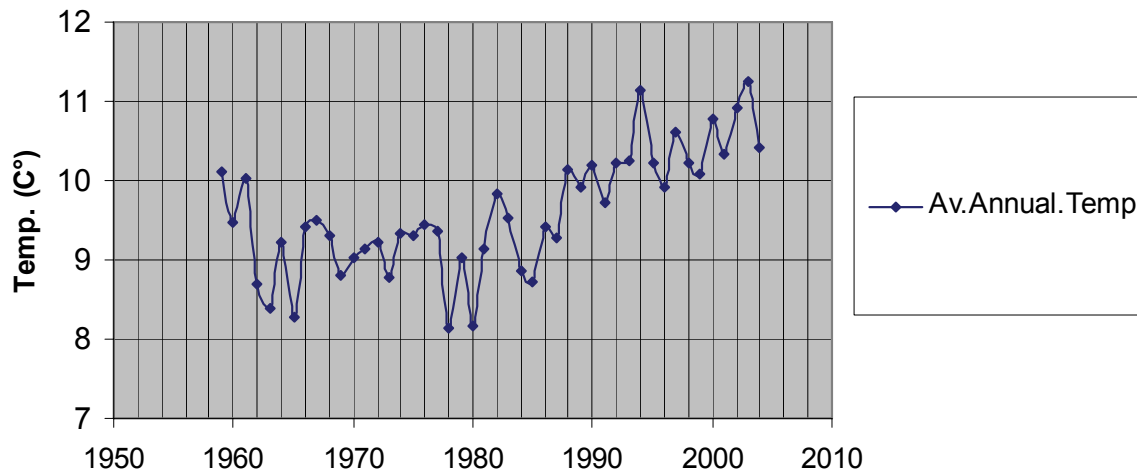


Figure 11.2.: There is a clear increase in temperature over the considered time span. The temperature differences spreads over the whole year but the summer temperatures increase faster (MeteoSchweiz).

In addition to the minimal estimation of the sediment degradation (active area) during the last decades, which is higher than what was exported in the last years, it is clearly recognizable that a sediment entrepot has built over the last decades. This suggests that sediment discharge in the Illgraben catchment is transport-limited, and that the installation of a warning system that considers threshold precipitation conditions for flow initialization should be possible.

### Implications for the morphology of the Rhône valley

Galloway and Hobday (1983) showed a relationship between the flow pattern of a river and the relative importance of bedload. Specifically, increasing bed load in relation to the total load, increasing sediment size, a higher flow velocity and a higher gradient of the channel bed will result in a change from a straight channel to a meandering channel and then to a braided flow pattern. Also, the relative bar stability decreases from the situation of a straight channel to that of the braided river, because stream power increases. The ratio of bedload to total-load changes strongly at the confluence of the Illgraben with the Rhône, because there is a substantial sediment influx. Furthermore the grain size distribution curves show a shift to much coarser grain sizes. Also, the gradient of the longitudinal stream profile of the Rhône increases distinctly after the confluence of the Illgraben. On the aerial photographs it is clearly recognizable that the Rhône had a

meandering flow pattern above the confluence before the first Rhône-correction was completed between 1863 and 1893. Further downstream, the Rhône is still in its natural state and shows a braided flow-pattern. This shows that sediment flux of the Illgraben has had a strong impact on the flow pattern of the Rhône and on the geomorphology of the valley.

## 6. Conclusions

The photogrammetric analysis yielded a sediment discharge over the last 45 years that is in the same order of magnitude as the discharge that has been measured since 2000 (Table 1 & 2). This was to be expected because the precipitation data does not show any trend to higher rates nor is there evidence to higher intensities (Fig. 11.1). 2006 was a very active year, and sediment discharge revealed a two fold increase. A temperature increase that was observed over this time period could be the reason for this higher discharge due to melting permafrost on the north face of the Illhorn (Fig.11.2). In summer 2006 it was observed that this new sediment source initiated channels beneath the Illhorn (Fig 6).

The built up of the sediment storage in the channel is strong evidence to infer a transport-limited system in terms of sediment flux. Such a system cannot export all supplied sediment (Fig. 4).

The Illgraben retains the Rhône. This can be seen on the longitudinal stream profile of the Rhône which shows an inflection point in the area of the confluence with the Illgraben (Fig. 7). Channel sediments above the confluence are much finer grained than beneath it, and the flow pattern changes from a meandering river to a braided river (Table 3.1, Fig. 7 & 8). Oxbow lakes with a high sinuosity and scroll bars in the inner side of the meander loop are still recognizable above the confluence (Fig. 10). Downstream of the confluence the Rhône shows a braided flow pattern (Fig. 7). The Illgraben sediment discharge has thus a direct influence on the flow pattern, stream gradient and grain size distribution of the Rhône.

## **Acknowledgments**

The scanning of the images was performed at FLOTRON AG in Meiringen (CH) which also supported this work with technical advices.

Corina Gwerder a master student from the ETH supervised by Brian McArdell collaborated with me and digitized the coupling/decoupling system which I used in this work.

The WSL made all information available that I needed. A special thank also to Brian McArdell who was on a fieldtrip together with Fritz Schlunegger and me.

## References

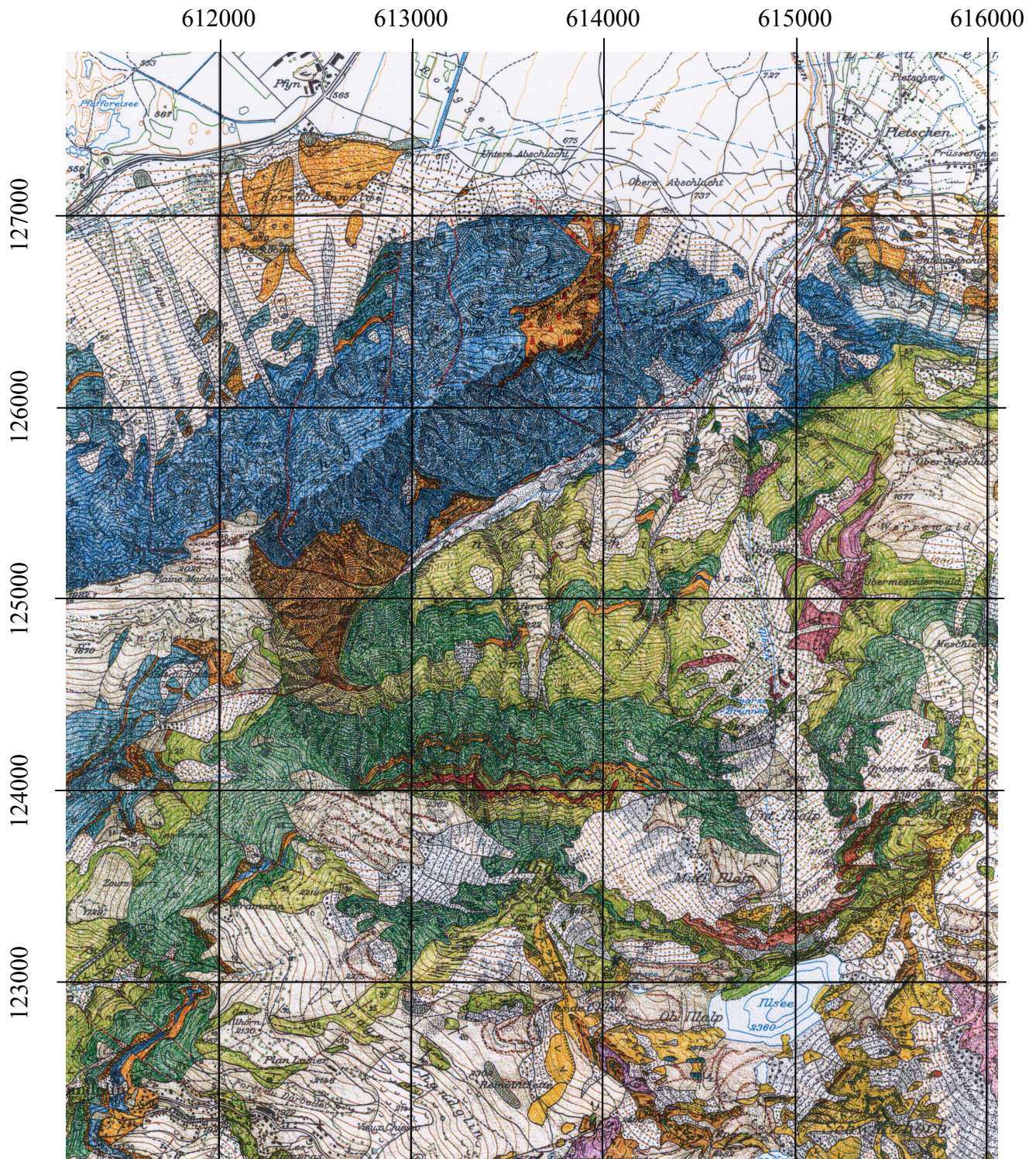
- Bovis, M.J. & Jakob, M. (1999) The role of debris supply conditions in predicting debris flow activity. *Earth surface processes and landforms* 24, 1039 – 1054.
- Buller, A.T. & McManus, J. (1979) Sediment sampling and analysis. In: *Estuarine Hydrography and Sedimentation* (Ed. By K.R. Dyer), pp. 87-130. Cambridge University Press.
- Folk, R.L. (1974b) *Petrology of Sedimentary Rocks*. Hemphill, Austin.
- Galloway, W.E. & Hobday, D.K. (1993) *Terrigenous clastic depositional systems*. Springer, Berlin, 423 pp.
- GEO7. 2001. *Geomorphologische Analyse des Illgrabens*, Bundesamt für Wasser und Geologie (BWG), Biel, Switzerland.
- Goudie, A.S. (2006) Global warming and fluvial geomorphology. *Geomorphology*, 79: 384-394.
- Graf, C. & McArdell, B. (2004) Murgangwaage – Ergänzung der Beobachtungs- und Messstation im Illgraben, in FAN, A., ed.: Zürich, WSL
- Gruber, M., Leberl, F., (2001) Description and evaluation of the high quality photogrammetric scanner UltraScan 5000. *ISPRS Journal of Photogrammetry & Remote Sensing* 55: 313 – 329.
- Gwerder, C., (2007) Temporal and spatial variation of erosion processes in the Illgraben, an alpine debris flow catchment. Unpublished diploma thesis, pp 1 - 102
- Hürlimann, M., Rickenmann, D. & Graf, C. (2003) Field and monitoring data of debris-flow events in the Swiss Alps. *Can. Geotech. J.* 40, 161 -175.

- Kääb, A., (2002) Monitoring high-mountain terrain deformation from repeated air- and spaceborne optical data: Example using digital aerial imagery and ASTER data. *Journal of Photogrammetry & Remote Sensing* 57, 39 – 52.
- Kääb, A., Huggel, C., Fischer, L., Guex, S., Paul, f., Roer, I., Salzmann, N., Schlaefli, S., Schmutz, K., Schneider, D., Strozzi, T., Weidmann, Y. (2005) Remote sensing of glacier- and permafrost-related hazards in high mountains: An overview. *Natural Hazards and Earth System Sciences* 5: 527 – 554.
- Krumbein, W.C. & Pettijohn, F.J. (1961) *Manual of Sedimentary Petrography*. Appleton-Century-Crofts, New York.
- McArdell, B.W., Bartelt, P. & Kowalski, J. (2007) Field observations of basal forces and fluid pore pressure in a debris flow, *Geophysical Research Letters*, 34, L07406, doi:10.1029/2006GL029183.
- McManus, J. (1988) Grain size determination and interpretation. *Techniques in Sedimentology* edited by Maurice Tucker pp. 63-85.
- Mikhail, E.M., Bethel, J.S., McGlone, J.C. (2001) *Introduction to modern photogrammetry*. John Wiley & Sons, New York.
- Rickenmann, D. (2001) Simulation des Fliessverhaltens, in M. Hürlimann, C.G., D. Näf, ed.: *Birmensdorf (Zürich), WSL*, p. 58.
- Rickenmann, D., Hürlimann, M., Graf, C., Naef, D. & Weber, D. (2001) *Murgang-Beobachtungsstationen in der Schweiz: "Wasser, Energie, Luft"*, 5401 Baden (Schweiz), v. 93, p. 1-8.
- Rickenmann, D. & Koch, T. (1997) Comparison of debris flow modeling approaches. In *Proceedings of the 1<sup>st</sup> International Conference on Debris-Flow Hazards Mitigation: Mechanics, Prediction and Assessment*, San Francisco, California. Edited by C.L. Chen, American Society of Civil Engineers (ASCE). pp. 576 – 585.

- Rickenmann, D. & Weber, D. (2000) Flow resistance of field and experimental debris flows in torrent channels. In Proceedings of the 2<sup>nd</sup> International Conference on Debris-Flow Hazards Mitigation: Mechanics, Prediction and Assessment, Taipei, Taiwan. Edited by G.F. Wieczorek and N.D. Naeser. A.A. Balkema, Rotterdam. pp. 245 – 254.
- Rickenmann, D. & Zimmermann, M. (1993) The 1987 debris flows in Switzerland: documentation and analysis. *Geomorphology* 8, 175 – 189.
- Schlunegger, F., Matter, A. & Mange, M. A. (1993) Alluvial fan sedimentation and structure of the southern Molasse Basin margin, Lake thun area, Switzerland. *Eclogae Geologicae Helveticae* 86.3 p 717-750.
- Schwab, M., Rieke-Zapp, D., Schneider, H., Liniger, M., Schlunegger, F. In press
- Swiss Federal Office for Water and Geology. 1999. Hydrological atlas of Switzerland. Federal Office for Water and Geology, Biel.
- Tognacca, C. (2000) Murgangentstehung im Gerinne. Mitteilung der Versuchsanstalt für wasserbau, Hydrologie und Glaziologie, ETH Zürich, Nr. 164, 259 pp.
- VAW (1992) Murgänge 1987: Dokumentation und Analyse. Unpublished Report. No. 97.6, Versuchsanstalt für Wasserbau, Hydrologie und Glaziologie (VAW), ETH Zürich, 620 pp.
- Vischer, D.L. (2003) Die Geschichte des Hochwasserschutzes in der Schweiz. - Von den Anfängen bis ins 19. Jahrhundert. Berichte des BWG, Serie Wasser – Rapports de l'OFEG, Série Eaux – Rapporti dell'UFAEG, Serie Acque Nr. 5 – Bern, 100 pp.
- Zimmermann, M., Mani, P. & Romang, H. (1997a) Magnitude-frequency aspects of alpine debris flows in China. *Natural Hazards* 7, 1 – 23.

## Appendix

Geological map of the Illgraben (WSL)



ZONE HOUILLERE ET NAPPE DES PONTIS

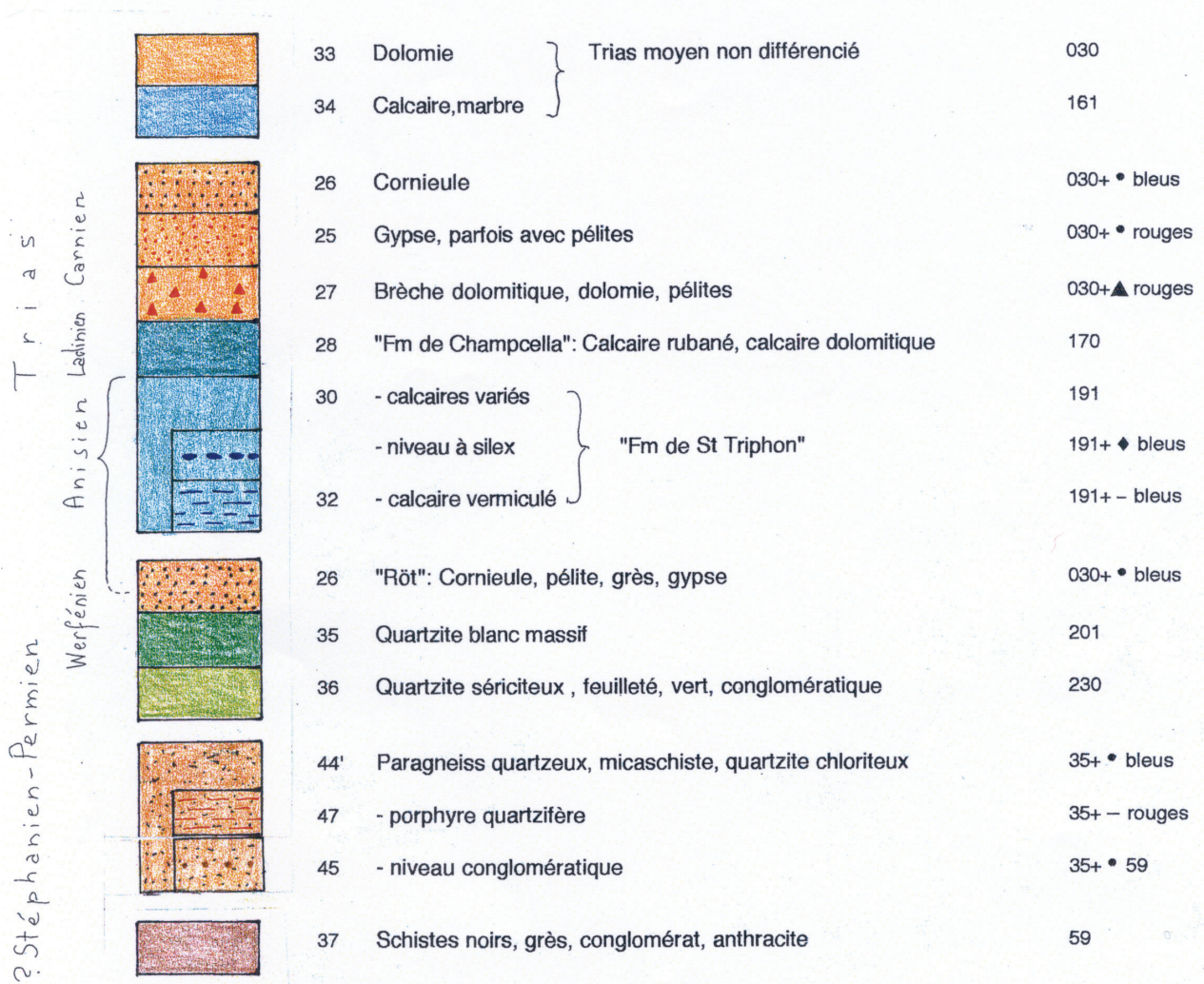


**Tabelle mit den Korngrößenverteilungen der vier untersuchten Sandproben aus dem Rhônebett. P1 und P2 wurden oberhalb des Illgrabenzuflusses genommen. P3 und P4 unterhalb davon.**

P1

Korngrösse (mm)	Gewicht (g)	Gewicht (%)	Summe-Gew-%
> 2	0.018	0.003	0.003
2 – 1.4	0.009	0.001	0.004
1.4 – 1.0	0.034	0.006	0.010
1.0 – 0.7	0.057	0.009	0.019
0.7 – 0.5	1.329	0.220	0.239
0.5 – 0.35	24.014	3.978	4.217
0.35 – 0.25	169.020	28.000	32.217
0.25 – 0.175	226.322	37.493	69.710
0.175 – 0.125	101.098	16.765	86.475
0.125 – 0.088	47.815	7.921	94.396
0.088 – 0.063	20.015	3.316	97.712
< 0.063	13.811	2.288	100.000

P2

Korngrösse (mm)	Gewicht (g)	Gewicht (%)	Summe-Gew-%
> 2	0.053	0.010	0.010
2 - 1.4	0.094	0.017	0.027
1.4 - 1.0	0.182	0.032	0.059
1.0 - 0.7	0.598	0.106	0.165
0.7 - 0.5	7.749	1.375	1.540
0.5 - 0.35	47.245	8.380	9.920
0.35 - 0.25	105.616	18.734	28.654
0.25 - 0.175	123.326	21.911	50.565
0.175 - 0.125	112.528	19.960	70.525
0.125 - 0.088	80.731	14.320	84.845
0.088 - 0.063	44.904	7.965	92.810
< 0.063	40.741	7.227	100.037

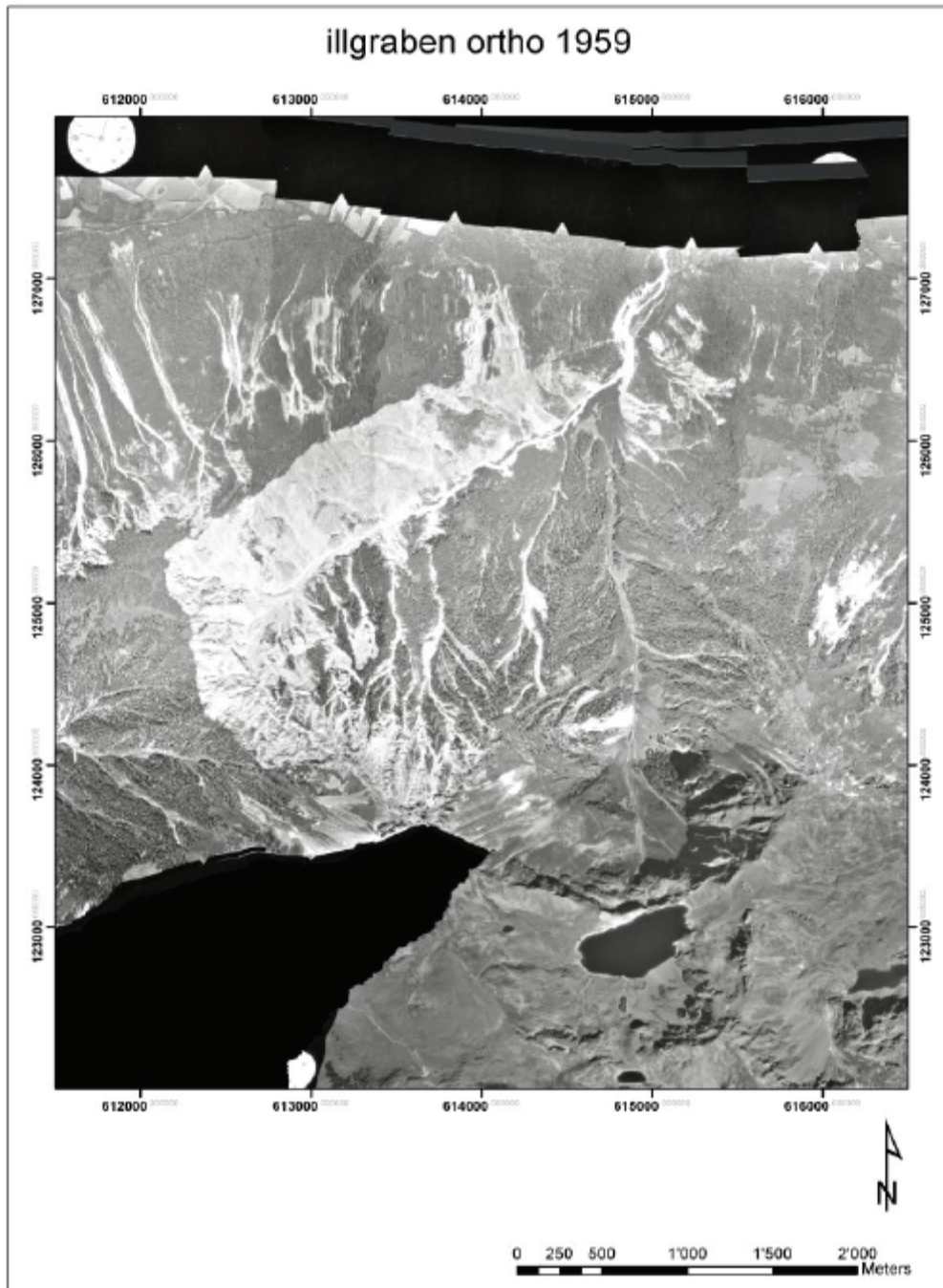
## P3

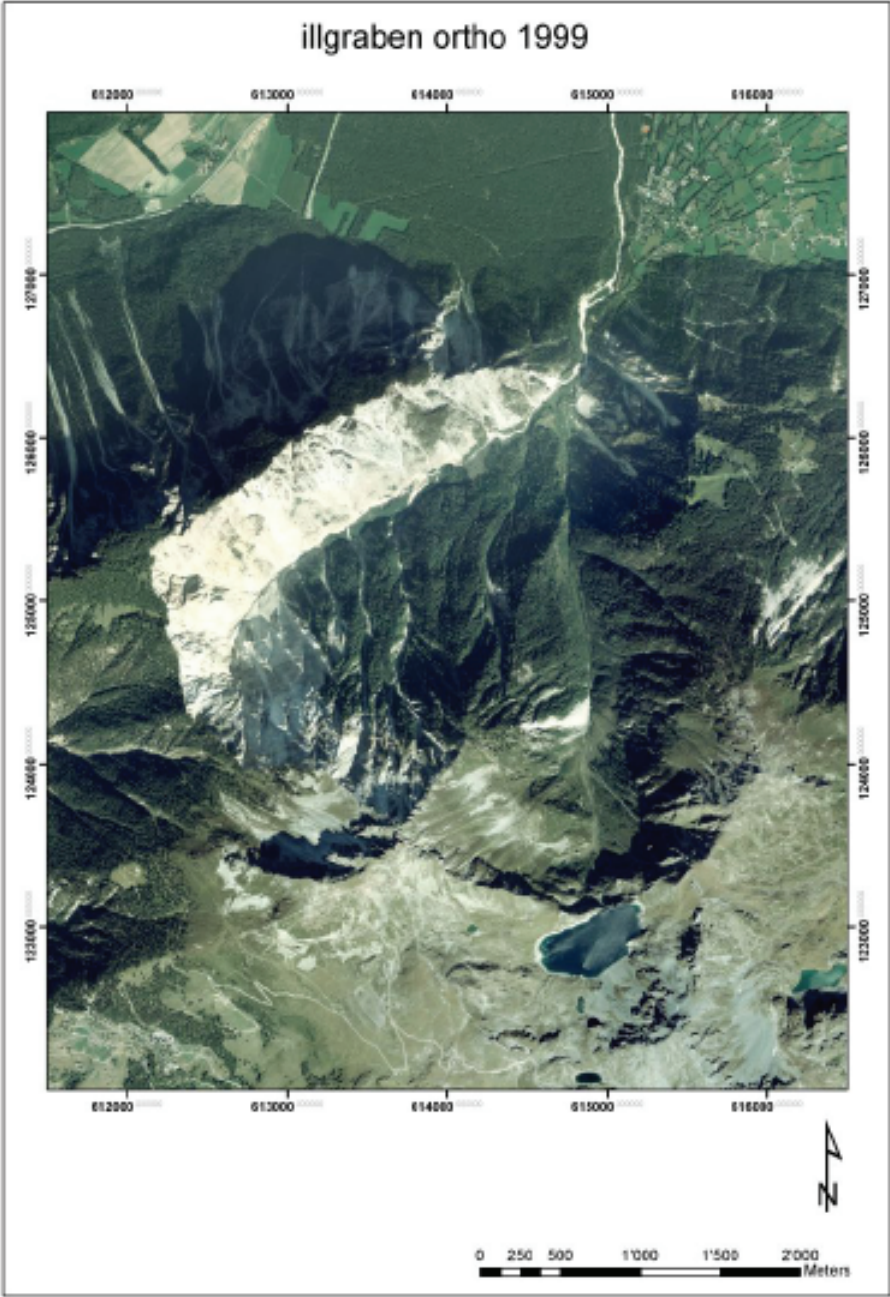
Korngrösse (mm)	Gewicht (g)	Gewicht (%)	Summe-Gew-%
> 2	7.610	1.332	1.332
2 - 1.4	12.801	2.241	3.573
1.4 - 1.0	37.452	6.556	10.129
1.0 - 0.7	73.649	12.893	23.022
0.7 - 0.5	144.778	25.345	48.367
0.5 - 0.35	135.788	23.771	72.138
0.35 - 0.25	92.589	16.209	88.347
0.25 - 0.175	46.842	8.200	96.547
0.175 - 0.125	14.821	2.595	99.142
0.125 - 0.088	3.767	0.659	99.801
0.088 - 0.063	0.506	0.089	99.890
< 0.063	0.626	0.110	100.000

## P4

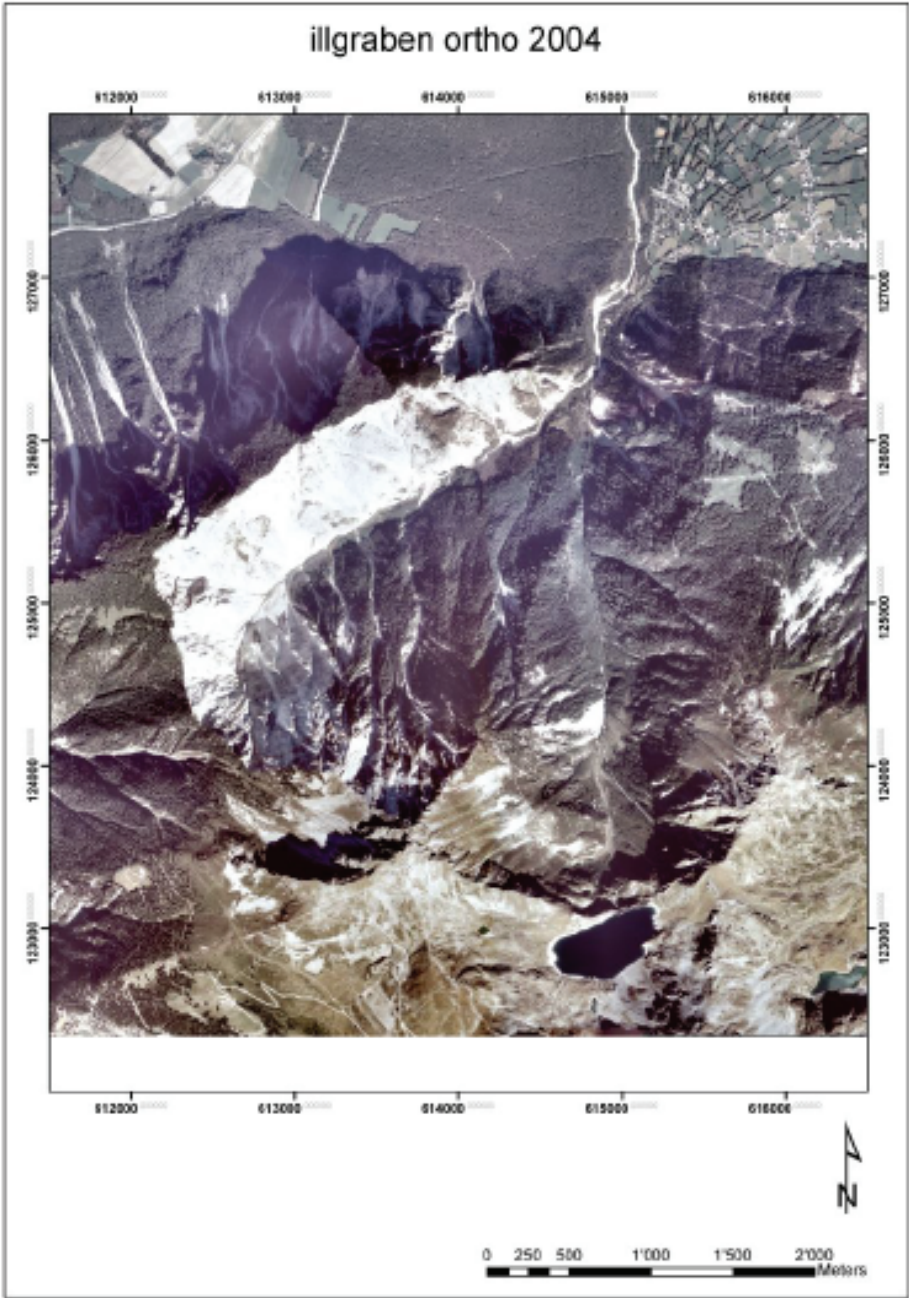
Korngrösse (mm)	Gewicht (g)	Gewicht (%)	Summe-Gew-%
> 2	12.729	1.868	1.868
2 - 1.4	21.027	3.085	4.953
1.4 - 1.0	65.328	9.586	14.539
1.0 - 0.7	113.943	16.720	31.259
0.7 - 0.5	162.128	23.790	55.049
0.5 - 0.35	108.080	15.859	70.908
0.35 - 0.25	67.033	9.836	80.744
0.25 - 0.175	45.638	6.697	87.441
0.175 - 0.125	40.762	5.981	93.422
0.125 - 0.088	26.008	3.816	97.238
0.088 - 0.063	11.855	1.740	98.978
< 0.063	6.956	1.021	99.999

**Selber erstellte Orthophotos von 1959 und 2004. Dazu das bereits vorhandene Orthophoto von 1999 (Swisstopo).**





Swisstopo



**Kameraprotokolle von Swisstopo zur internen Orientierung der Luftbilder**

## Kameraorientierungsprotokoll für die Luftbilder von 1959



---

### Calibration Certificate

**Wild Camera No.** 29



**Lens Cone**

Type: RC5  
 No.: 29  
 Size: 18x18 cm

**Lens Calibration date: 3.7.1**

Type: Aviogon  
 No.: 29  
 f= 115  
 max. aperture: f:5.6

**Resolving Power (Lines per millimetre)**

High contrast and max. aperture

	0°	5°	10°	15°	20°	25°	30°	35°	40°	45°
rad.	70	78	78	75	53	63	55	57	48	16
tang.	70	78	78	73	50	58	47	47	37	20

**Distortion in millimetres**

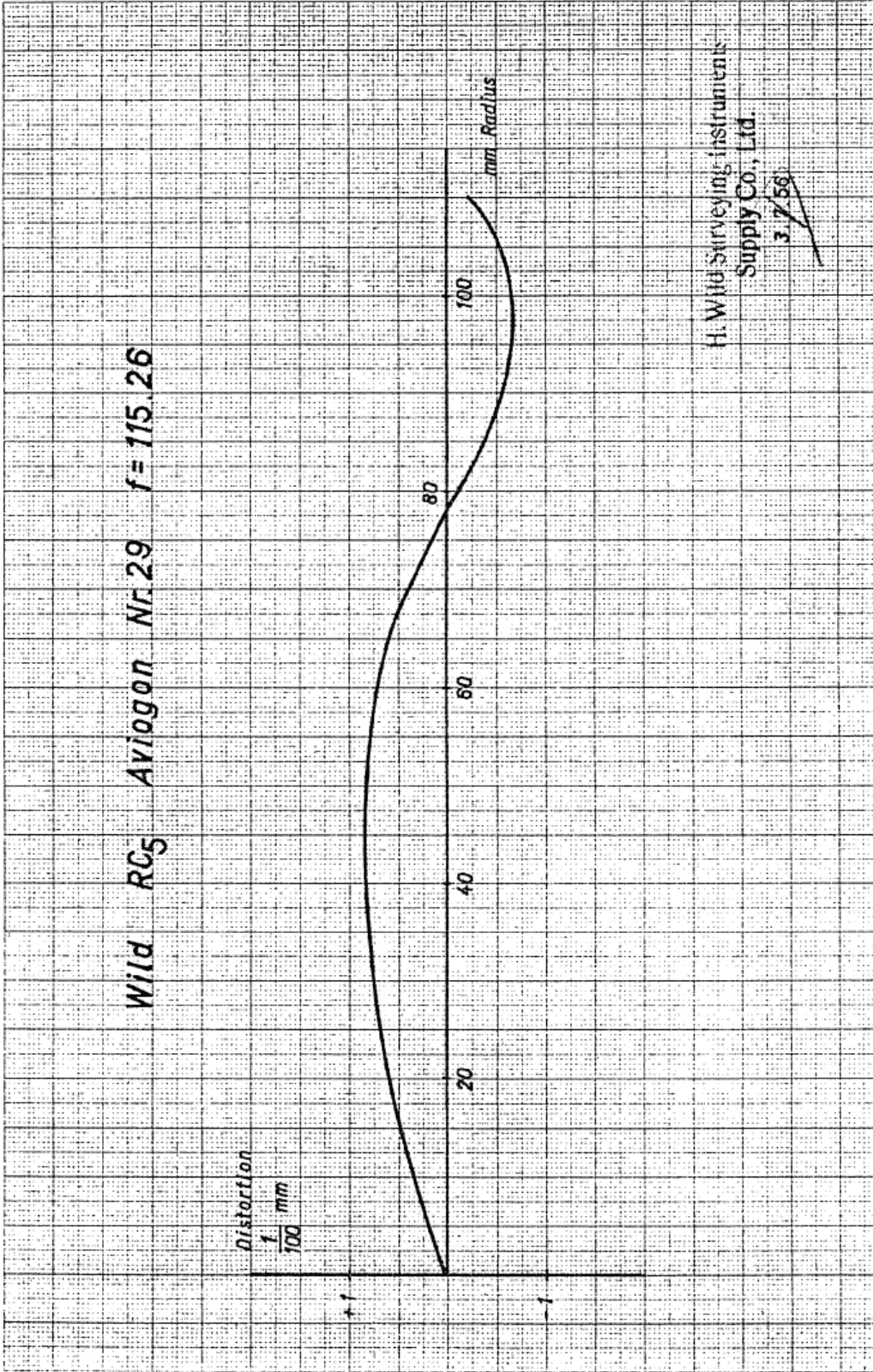
The given distortion is the arithmetic mean between the four half-diagonals. Positive distortion when away from the centre.

Calibrated focal length: 115.26

Radius	20	40	60	70	80	90	100	110
Distortion	+0.006	+0.008	+0.007	+0.004	-0.001	-0.006	-0.007	-0.002

The displacement of the optical centre from the intersection of the diagonals is within 0.01mm.

H. Wild Surveying Instruments  
 Supply Co., Ltd.



**LENS CONE**

Type: **BC5**  
No.: **11.5 Ag. 29**  
Size: **18 x 18 cm**

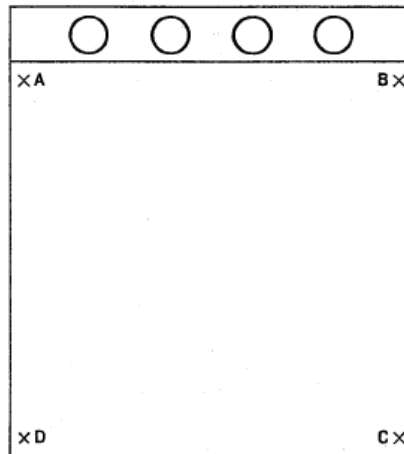
**LENS**

Type: **Aviagon**  
No.: **29**  
f = **115 mm**

**CALIBRATION DATE: 26.2.63**

*↓ NICHT VORHANDEN 1956*

Seen on camera from top



A — B = **163.993**  
B — C = **163.997**  
C — D = **163.992**  
D — A = **163.998**  
A — C = **231.929**  
B — D = **231.917**

WILD HEER RUGG  
*[Handwritten signature]*

**Kamerorientierungsprotokoll für die Luftbilder von 2004**

ca 1322002

**CAMERA CALIBRATION CERTIFICATE**

CAMERA TYPE : RC30  
LENS TYPE : 15/4 UAG-S  
LENS NO. : 13220

Calibration date: 04.06.2002

LEICA AG, HEERBRUGG

 **swissoptic**  
SwissOptic AG  
Heinrich-Wild-Strasse  
CH-9435 Heerbrugg  
Schweiz



9.7.02 a. g.

RC30

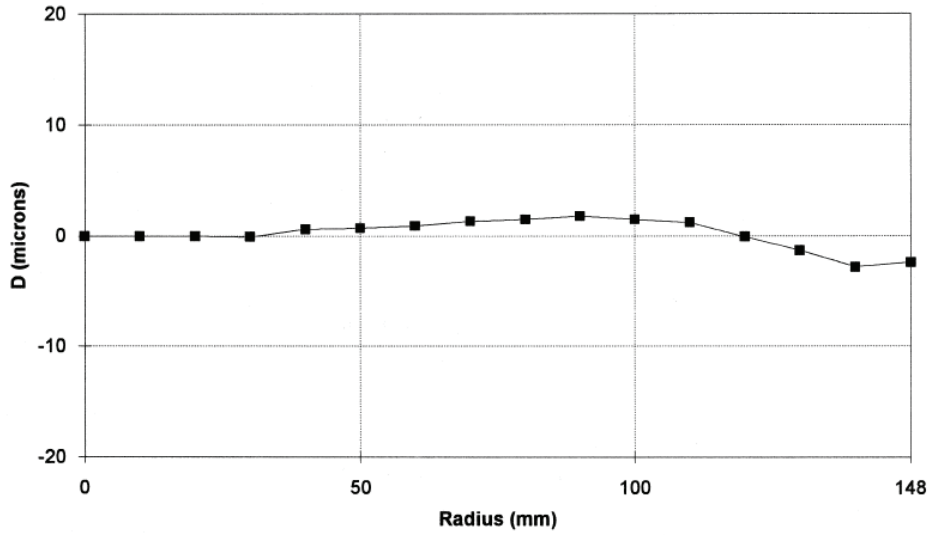
15/4 UAG-S

No. 13220

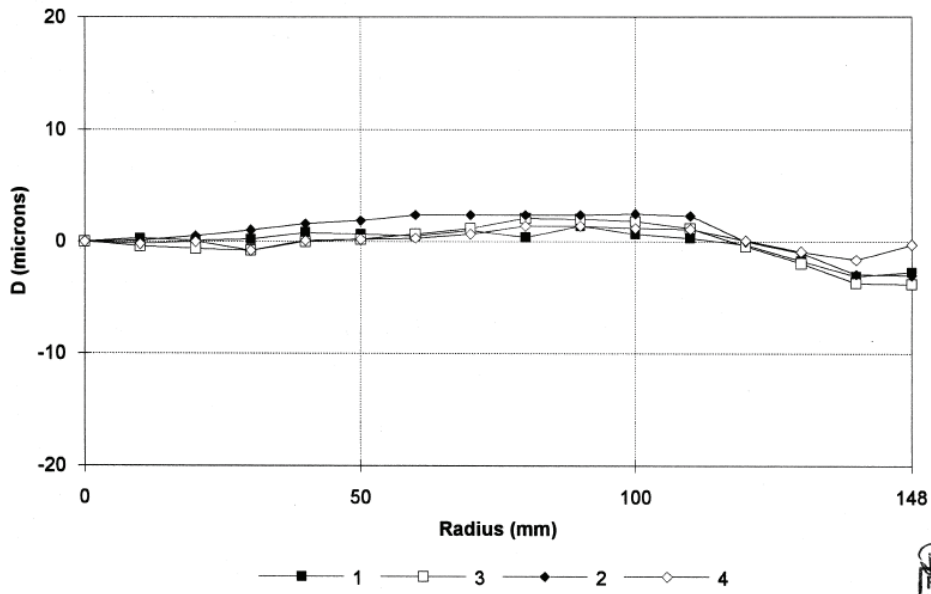
04.06.2002

Aperture: 4.0  
 Filter on goniometer: VIS (400-700 NM)  
 Filter on camera: --  
 C.F.L. : 152.51 mm

**Mean radial distortion**



**Radial distortion for semi-diagonals referred to PPS**



*David*  
 PO 066

RC30

15/4 UAG-S

No. 13220

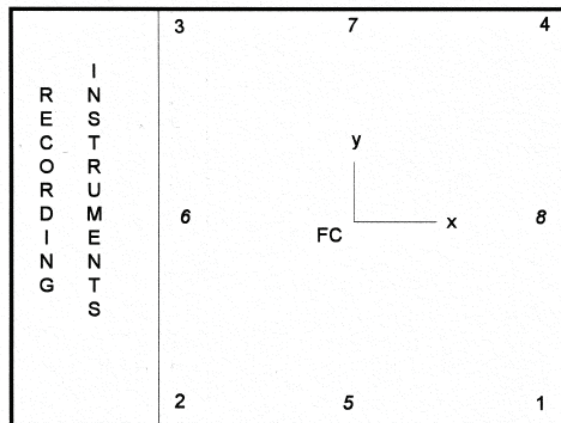
04.06.2002

**Principal point of autocollimation (PPA) and  
principal point of symmetry (PPS)**  
referred to central cross (FC), see diagram

	x (mm)	y (mm)
PPA	0.006	-0.002
PPS	-0.005	0.003

**Fiducial marks, referred to central cross (FC)**

	x (mm)	y (mm)		x (mm)	y (mm)
1	105.999	-106.000	5	-0.003	-111.999
2	-106.000	-106.003	6	-111.999	0.003
3	-106.002	106.003	7	0.000	112.006
4	106.003	106.006	8	112.002	0.003



as seen on focal plane frame



RC30

15/4 UAG-S

No. 13220

04.06.2002

Aperture: 4.0  
 Filter on goniometer: VIS (400-700 NM)  
 Filter on camera: --  
 C.F.L. : 152.51 mm

**Radial distortion (micrometers) referred to principal point of symmetry (PPS)**  
 (Positive values denote image displacement away from center)

Radius mm	Half - Sides				Mean
	1	3	2	4	
10	0.3	-0.4	0.1	-0.2	0.0
20	0.1	-0.6	0.5	0.0	0.0
30	0.2	-0.8	1.0	-0.8	-0.1
40	0.8	0.0	1.6	0.1	0.6
50	0.7	0.2	1.9	0.2	0.7
60	0.5	0.7	2.4	0.3	0.9
70	1.0	1.2	2.4	0.7	1.3
80	0.4	2.1	2.4	1.4	1.5
90	1.4	2.0	2.4	1.4	1.8
100	0.7	1.8	2.5	1.2	1.5
110	0.3	1.2	2.3	1.1	1.2
120	-0.3	-0.4	0.0	0.1	-0.1
130	-1.7	-1.9	-1.0	-0.9	-1.3
140	-3.1	-3.7	-2.9	-1.6	-2.8
148	-2.7	-3.8	-3.0	-0.3	-2.4

**Photographic resolution (line pairs per millimeter)**

International 3-line test-chart, contrast (log) : 2.0  
 Aperture: 4.0  
 Filter: 450 NM  
 Film: KODAK PANATOMIC X 2412  
 Developer: KODAK HC110

Angle (deg)	0	5	10	15	20	25	30	35	40	45
Radial:	117	117	103	101	98	95	114	108	101	83
Tangential:	117	104	90	87	103	96	88	88	87	66

AWAR (Area weighted average resolution) in lp/mm: 97

